Chapter 1

Introduction and Literature Review

1.1 Introduction

The carbon-emission free energy necessity of the world is on the rise to avoid the environmental pollution and emission of greenhouse gases. Ecological destruction and environmental pollution generated from fossil fuels forced industry and scientific community to search for carbon emission-free energy. Solar power has attracted much attention because it's non-polluting, renewable and comes from the sun as an unlimited energy source. Photovoltaic cells based on crystalline silicon, Copper indium gallium selenide and Cadmium telluride are efficient, but their production process is costly. Thus it becomes an urgent need to develop thin film-based devices that require low cost materials and their development process is easy and cheap. In order to trim down the energy harvesting expenditure, several efforts have been made to substitute crystalline silicon photovoltaic devices with thin film photovoltaic devices.

In recent years, solar cell based energy solutions have got tremendous attention due to carbon emission-free energy technology for protection of the environment. High efficiency Solar cells based on organometal-halides with perovskite structures have motivated to study the photovoltaic phenomena in oxide perovskite materials also [P. X. Gao et al. (2003)]. After the motivating discovery of high-voltage photovoltaic (PV) effect in $LiNbO_3$ and $BaTiO_3$; and their potential to exceed the highest reported efficiency, energy harvesting devices using ferroelectric perovskite oxide materials have attracted as an alternative to traditional silicon solar cells; owing to very good chemical stability, low cost, abundance in nature and higher photovoltage [S. Y. Yang et al. (2010)]. Various Ferroelectric perovskite oxide such as $BaTiO_3$, $PbTiO_3$, $Pb(Zr,Ti)O_3$, $BiFeO_3$, were investigated and have shown considerable ferroelectric photovoltaic effect[A. M. Glass et al. (1974); P. S. Brody et al. (1975); Z. Tang et al. (2014); B.

Chen et al. (2012)]. To date, the power conversion efficiency of ferroelectric photovoltaics is not good enough to satisfy the commercial applications and more research and development work are required. The reason behind low power conversion efficiency of ferroelectric perovskites is the low light to electrical energy conversion efficiency due to the wide band gap of these materials which limits the light absorption in photoactive layer [H. Zhou et al. (2014)]. Various studies have focused chemical doping as an efficient method to lower the band gap of perovskites to improve the photocurrent response [H. An et al. (2016)]. Different types of the donor and acceptor dopants have been used for lowering the optical band gap of $PbTiO_3$, which can be done by doping either at A-site(Pb) or B-site(Ti) in ABO_3 perovskite structure of $PbTiO_3$ [W. Zhou et al. (2016)]. Moreover, strain engineering of perovskite oxides by methods like thin film deposition etc. are also being adopted to shrink the optical band gap [H. Matsuo et al. (2017); W. S. Choi et al. (2012); X. Yuan et al. (2019); L. You et al. (2018)]. Recently, ferroelectric films of $BiFeO_3$ and $Pb(Zr,Ti)O_3$ have been reported for photovoltaic response. Katiyar et al. reported photoresponse of the $BiFeO_3/SrRuO_3$ heterostructure with 63 μ A/cm^2 short-circuit current density (J_{sc}) [R. K. Katiyar (2014)]. Cao et al. depicted J_{sc} ~ 4.8mA/cm^2 for PZT thin films based ferroelectric solar cells [D. Cao et al. (2012)]. There is increased J_{sc} ~12.1 mA/cm^2 reported for Nd-doped BFO thin films by Ukai et al. [Y. Ukai et al. (2012)]. Recently, a double perovskite Bi_2FeCrO_6 with low band gap of ~1.2 eV has been reported which exhibits photovoltaic response [R. Nechache et al. (2011)]. Results reported by Nechache et al. led to the design of a new class of ferroelectric photovoltaic materials.

In view of the foregoing, the development of low band gap multiferroic/ferroelectric ceramics with high spontaneous polarization is the need of hour to develop high efficiency economical solar cells. The present thesis deals with the investigation of

many perovskite ferroelectric/multiferroic solid solutions namely, $PbTiO_3$-$Bi(Ni_{2/3}Nb_{1/3})O_3$, $Bi(Co_{1/2}Ti_{1/2})O_3$-$PbTiO_3$, $Bi(Ni_{2/3}Nb_{1/3})O_3$-$BaTiO_3$, $KNbO_3$-$Ba(Ni_{1/2}Nb_{1/2})O_3$, $KBiFe_2O_5$ and $RFeO_3$. The developed materials were characterized for band gap, ferroelectric, dielectric and photovoltaic behavior as a function of composition in bulk and thin film forms. Before starting discussion about important findings and results of this thesis in subsequent chapters, we will recap the basic concepts related to ferroelectric photovoltaics in perovskite oxide materials. The later part of this chapter presents a brief review of the existing literature on ferroelectric photovoltaic materials. The literature on $BiFeO_3$, $PbTiO_3$, $BaTiO_3$ and $KNbO_3$ based binary solid solutions, which show photovoltaic behaviour, is reviewed at the end of this chapter.

1.2 Perovskites Structure

Gustav Rose discovered a mineral calcium titanate in 1839 and named it "perovskite" in honour of the Russian mineralogist Lev Perovski [L. J. Schmidth (2011)]. Later, Victor M. Goldschmidt studied the crystal structure of calcium titanate ($CaTiO_3$) [V. M. Goldschmidt (1926)]. The crystal structure of perovskite follows the general formula ABO_3 (or ABX_3) where the letters 'A' and 'B' stand for the two cations with total ionic charges +6 and 'O' is generally a divalent anion like oxygen, as shown in Fig 1.1(a). In the cubic unit cell of perovskite crystal structure, the corner positions of the cube are occupied by A-cations while B-cations reside in the body-centre position. Oxygen anions are situated at face-centred positions. The stability of perovskite structure in ABO_3 type ionic solids is predicted by tolerance factor first suggested by Goldschmidt [V. M. Goldschmidt (1926).] Geometrical considerations for ABX_3 cubic perovskite unit cell with A-occupying cube corners, B-occupying body centre and X (or O)-occupying face centres leads to the following equation for the tolerance factor 't',

$$t = \frac{R_A + R_X}{\sqrt{2}(R_B + R_X)} \qquad \ldots\ldots\ldots\ldots\ldots\ldots \quad (1.1)$$

Where R_A, R_B and R_X are the ionic radii of A-site cation, B-site cation and X (or O) anion, respectively [C. A. Randall et al. (1990)]. For ideal cubic perovskite structure, the tolerance factor t = 1, however, stability of perovskite structure can be also seen in the range $0.80 < t < 1.1$. The deviation of tolerance factor from 1, leads to distortion of cubic structure and appearance of non-cubic structures like tetragonal, rhombohedral, orthorhombic, hexagonal, monoclinic etc. ABO_3 type perovskite oxides with various B-site doping have been comprehensively studied to optimize appropriate physical properties, for instance, ferroelectricity, ferromagnetism, and band gap in the product phase. Fig 1.1(a) shows the crystal structure of cubic ABO_3 perovskite oxides with space group Pm3m. In ideal condition, ABO_3 cubic perovskite structure consists of a 3-D frame work of corner-sharing BO_6 octahedron and the A-site cation occupy the 12 coordinate cavities formed by BO_6 network and is surrounded by 12 equidistant oxygen ions [C. Li et al. (2004)].

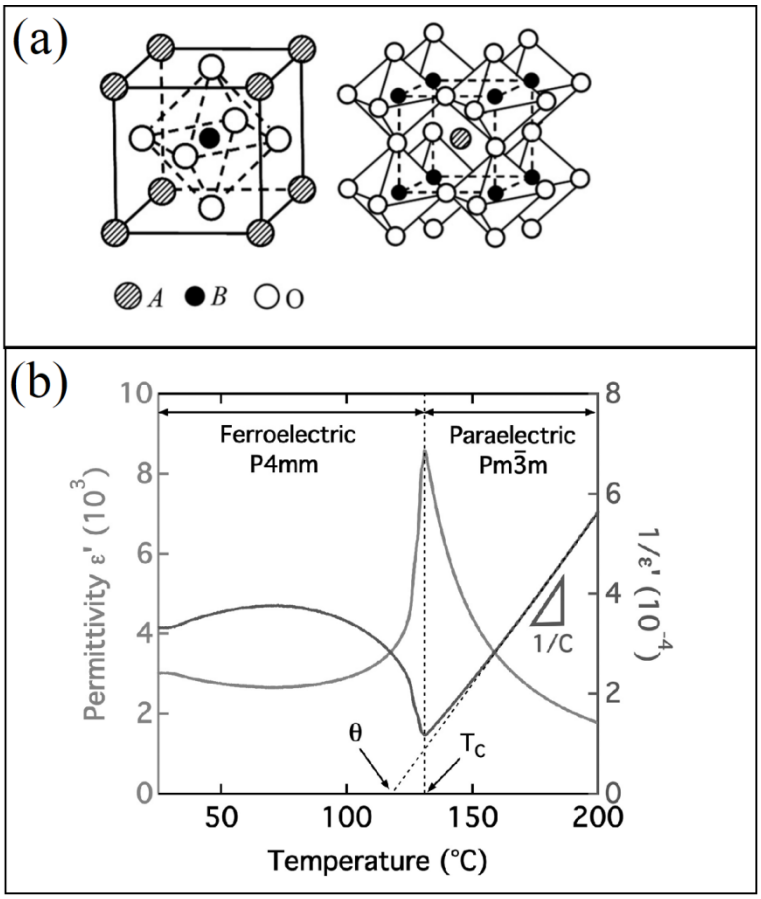

Figure 1.1 (a) Representation of crystal structure of cubic perovskite oxides ABO_3 (N. Xu et al 2010) (b) Typical dielectric constant vs. temperature plot for ferroelectric to paraelectric transition in $BaTiO_3$ [F. H. Schader et al. (2013)].

1.3 Ferroelectricity and related phenomena

Ferroelectricity is a physical property of specific materials which possess spontaneous electrical polarization that is reversible upon application of an external electric field. The ferroelectricity phenomenon can exist in non-centrosymmetric materials only. A ferroelectric material is defined as a material which exhibits a spontaneous electric dipole moment even in absence of an applied electric field. The spontaneous polarization is caused by the relative ionic displacements in the non-centrosymmetric crystal structure. The spontaneous polarization depends on the position of the ions or on the charge ordering of multiple valences. The spontaneous polarization

is steady under a broad range of chemical and thermal conditions. At a characteristic high temperature, called as Curie temperature, the spontaneous polarization of the materials with non-centrosymmetric crystal structure is lost due to conversion into centrosymmetric structure, mostly cubic in case of perovskites. The high temperature phase is called as paraelectric phase and temperature dependence of dielectric permitivity exhibits a peak at the ferroelectric to paraelectric phase transition temperature as shown in Fig 1.1 (b). The ferroelectric materials are pyroelectric and piezoelectric, but the reverse is not possible. The ferroelectric solid systems demonstrate high dielectric permittivity and piezoelectricity. If any material consists of spontaneous polarization and have confirmed re-orienting of the polarization, only then it is called as ferroelectric material.

In principle, ferroelectric materials possess a polarization (P)-electric field (E) hysteresis loop as a characteristic fingerprint. Fig. 1.2 illustrates a usual P-E hysteresis loop. From P-E loop, various parameters such as remnant polarization (P_r), spontaneous polarization (P_s) and coercive field (E_c) can be determined [L. Jin et al. (2014)]. In polycrystalline materials the grains split into many domains, which are randomly distributed in such way that material shows zero net macroscopic polarization. When applied external electric field strength exceeds the coercive field (E_c) of the material, the ceramic may reach in the polar state. When applied external field strength starts to decrease, some domains will switch back, still at zero electric field, the net polarization is not reach to zero, which is called the remnant polarization (P_r).

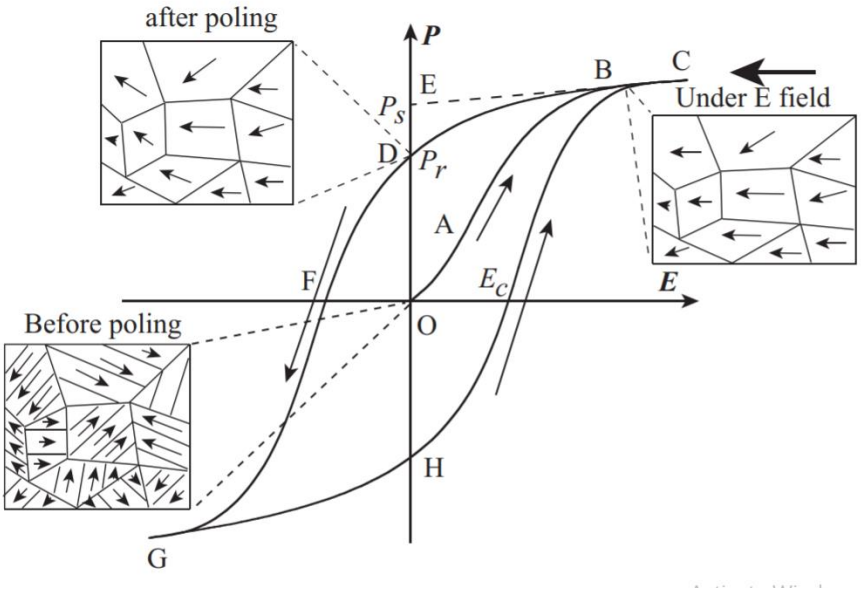

Figure 1.2 Typical P-E hysteresis loop for ferroelectric materials [L. Jin et al. (2014)].

The region in which spontaneous polarization is unidirectionally oriented in ferroelectric material, is called ferroelectric domains, and these domains are separated by a plane called domain wall. The width of domain walls is of few nm ranges. The formation of domains in ferroelectric materials happens to minimize the depolarization field in the material itself [D. D. Fong et al. (2006)].

The ferroelectricity in perovskites may originate due to either cation-displacements or presence of lone-pair electrons or special geometry leading to non-coincident centres of positive and negative charges. In $BaTiO_3$, the ferroelectricity originates by Ti-ion off-centring in the oxygen ion octahedral cage. The Ti-ion off-centring creates distortion in crystal structure and thus spontaneous polarization arises in the $BaTiO_3$. Ferroelectricity in $BiFeO_3$ is due to the presence of lone pair electrons (S^2) of Bi^{3+}. The S^2 lone pair electrons shifts the Bi^{3+} to generate the spontaneous polarization [Catalan and Scott (2009)]. In $BiFeO_3$, the ferroelectricity arises from on-site sp re-hybridization of the two 6s electrons of Bi^{3+} that do not participate in the chemical bonding [P. Barone et al. (2015)].

The lead based ferroelectric materials show higher ferroelectricity due to the presence of Pb^{2+} ions, which have lone-pair $6s^2$ electrons. The lone pair $6s^2$ electrons lead to off-cantering of Pb^{2+} in the cage of oxygen neighbours. Cohen et al have reported that $6s^2$ electrons contribute to ferroelectricity as they hybridize with the oxygen 2p states and result in a substantial spatial shift of Pb^{2+} ions and the electron density [R. E. Cohen (1992); T. Egami (2007)]. In $PbTiO_3$-$BiMeO_3$ binary systems, the Bi^{3+} cation is considered very promising due to its ability to produce large spontaneous polarization and a high Curie temperature. For example, $PbTiO_3$-$BiScO_3$ has a high Curie temperature (450°C) and a large remnant polarization (P_r ~ 74μC/cm^2) [M. Yashima et al. (2011)].

1.4 Light induced physical phenomena in materials

When incident light is absorbed by a material, it raises the energy of the electrons and creates high-energy electrons within the material. The absorption of light and generation of photoelectrons process gives rise to phenomenon such as photoconductivity, Photo-Dember effect, photodielectric effect, photo-polarization, and photovoltaic effect. The opto-electronic phenomenon in which a material becomes more electrically conductive after absorbing light is called photoconductivity. When photons of electromagnetic radiation having energy equal to or more than band gap of material are absorbed by material, they generate the extra photo-electrons which results in enhancement of electrical conductivity. A photodetector is based on photoconductivity in semiconducting materials. A photodetector absorbs the light and converts the optical energy into the quantifiable electric current. The performance of photodetectors is decided by their photo-response sensitivity and photo-to-dark current ratio.

The photoconduction process is a combination of different transport phenomenon which occurs simultaneously. In the photoconduction process, first charge carriers are generated. These charge carriers go through recombination and transportation at the same time. Few charge carriers are recombined, and the rest are transported to the electrodes. Charge carriers' statistics, thermal and hot carrier relaxation process, and effects of electrodes are also involved in the photoconduction process [N. V. Joshi (1990)]. The concept of photoconduction process is used in photo-detection and radiation measurements. The photoconduction mechanism is illustrated in Fig 1.3. Under light illumination, when photons have energy equal to or more than the band gap of the material, electrons and holes are created in the conduction band and valence band, respectively and increase the conductivity of material [E. P. Mukhokoshi et al. (2020)]. In doped materials, photoconduction phenomenon take place due to excitation near the band edge and even photons with energy less than band gap of that material can increase its photoconductivity. Photoconduction process involve various transitions such as impurity levels to band edge, Band-to-Band, ionization of donors and deep levels situated in valance band (V.B.) to conduction band (C.B.) [V. M. Fridkin et al. (1973)]. The current obtained due to photoexcited carriers is driven by the intrinsic polarization and defined by the equation:

$$J = (\sigma_d + \sigma_{ph})\, \xi \qquad \text{…….... ……..} \quad (1.2)$$

Where σ_d is conductivity in the dark and σ_{ph} is the light conductivity component while ξ is the electric field. If wavelength of incident light is equal to or more than the band gap of materials, the increase in photoconductivity is observed [S. R. Basu et al. (2008)]. Bhatnagar et al. (2014) have studied dark-light current (I)-voltage (V) characteristics of $BiFeO_3$ to explore if any improvement in conductivity happens under light illumination. They have reported enhanced photoconductivity in strained $BiFeO_3$ films under

illumination with light as shown in Fig 1.4. An increase in photoconduction is accredited to occurrence of sub-band levels within the band gap of $BiFeO_3$ which may be activated under light and contributes to the conduction mechanism [A. Bhatnagar et al. (2014)].

Due to different electron and hole mobilities, a voltage gradient is created in the direction of strongly absorbed electromagnetic radiation. It will create a difference in concentration of photo-excited holes and electrons with respect to position in the sample. This asymmetric diffusivity of photocarriers is called photo-Dember effect, and it will cause a transient spatial charge distribution and an electric field in the direction of light illumination [C. H. Liu et al. (2015)].

If change in capacitance is observed upon light illumination on dielectric of a capacitor, the phenomena is called photodielectric effect. Previously photodielectric effect was reported in photosensitive semiconductors such as ZnS, CdS, CdTe and ZnO etc. [P. Krispin et al. (1964)]. Various hypotheses were proposed to explain the origin of photodielectric effect. This effect was attributed to polarization of traps, the rising concentration of free charge carriers in an unevenly illuminated sample, space charge on the grain boundaries and change of nonequilibrium hopping conductivity in an alternating electric field [J. Webster (2001)]. T. Nagai et al. have reported light-induced increase of dielectric permittivity in $LaAl_{0.99}Zn_{0.1}O_{3-\delta}$ ceramic capacitor [T. Nagai et al. (2017)]. Fig. 1.5 shows the effect of light illumination on dielectric permittivity (ε′) and dielectric loss (tanδ) for $Ba(Al_{0.95}Zn_{0.05})_2O_{4-\delta}$. They have proposed that photodielectric effect is originated from dielectric response of combination of photo-induced electrons and holes present in deep gap states and at the non-dispersive valence band maximum (V.B.M) [T. Nagai et al. (2018)]. Y. Wei et al have reported an increase in permittivity from ~756 to ~807 under light illumination for $0.78Bi_{0.5}Na_{0.5}TiO_3$-$0.12BaTiO_3$-

$0.1Ba(Ti_{0.5}Ni_{0.5})O_{3-\delta}$ ceramic dielectric [Y. Wei et al. (2018)]. This effect can have important applications for designing the laser-controlled touch display, light-controlled capacitors etc. The difference between obtained I-V curve in conventional p-n junction photovoltaic effect, photoconductivity and bulk-photovoltaic effect is illustrated in Fig. 1.6 using schematic plots.

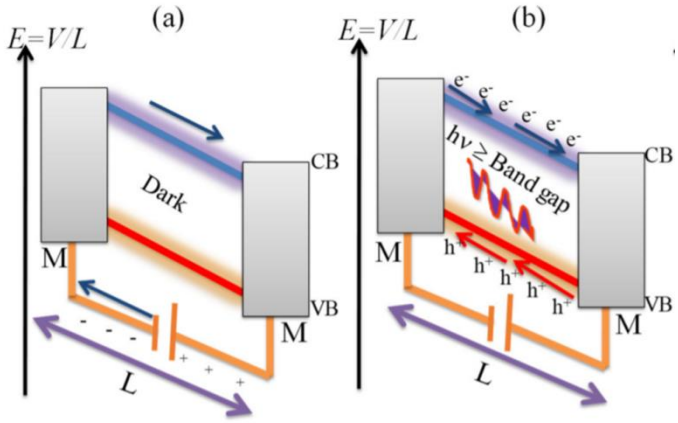

Figure 1.3 Schematic diagram of a photoconductor between two metal contacts (M) (a) in dark and (b) under illumination [E. P. Mukhokoshi et al. (2020)].

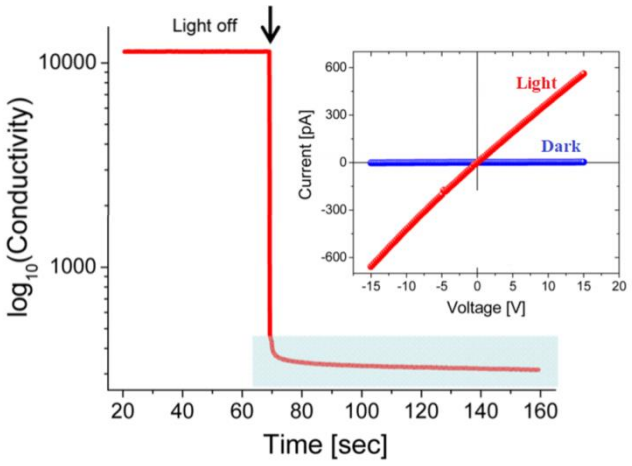

Figure 1.4 Logarithmic plot of conductivity with time. The inset shows IV curves obtained before (blue) and after (red) illumination for a $BiFeO_3$ film (A. Bhatnagar et al. (2014)].

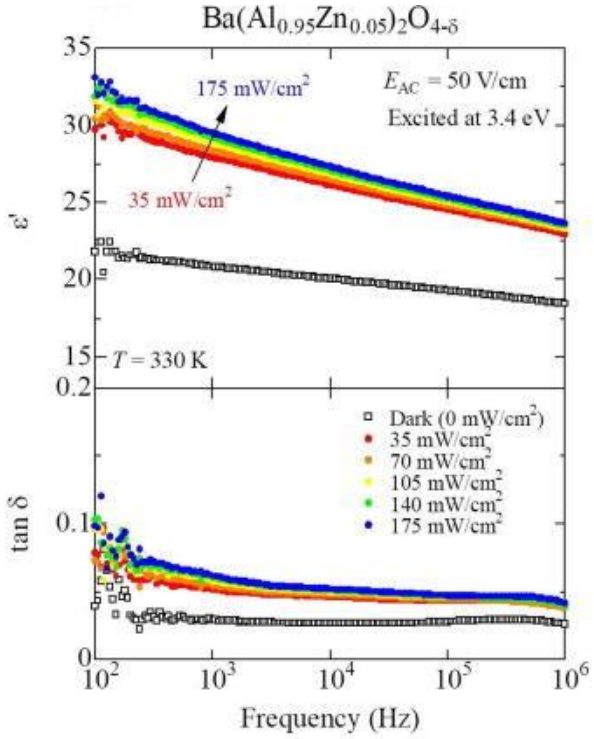

Figure 1.5 Frequency dependence of (a) dielectric permittivity and (b) dielectric loss (tanδ) at 330 K for $Ba(Al_{0.95}Zn_{0.05})_2O_{4-\delta}$. Squares and circles point out the dark states and the photo-irradiated states respectively. (T. Nagai et al. (2018)].

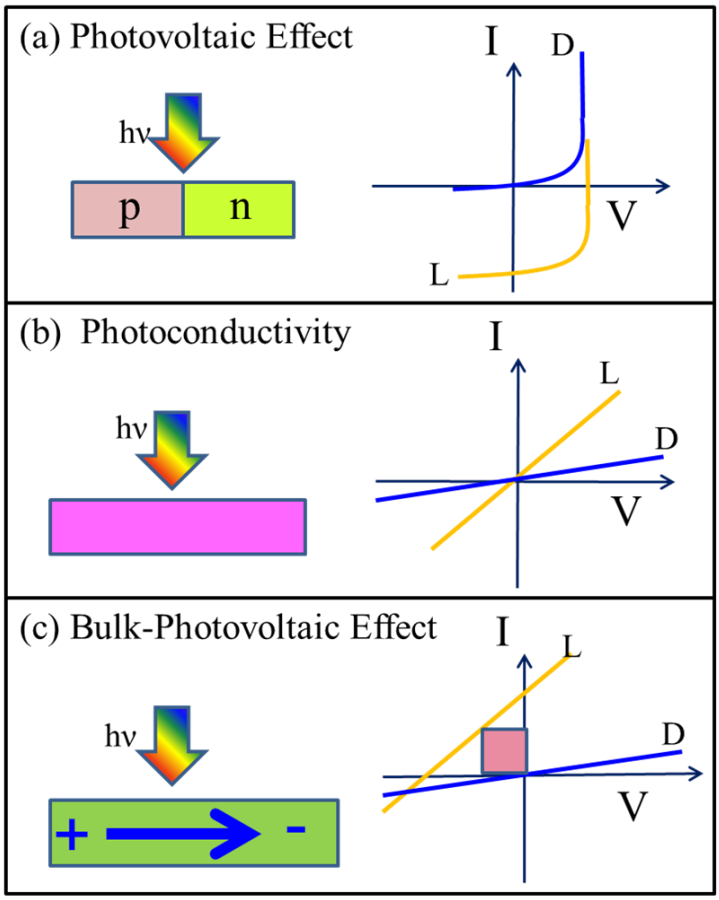

Figure 1.6 Typical schematic I-V diagrams for (a) photovoltaic effect (b) photoconductivity and (c) Bulk-photovoltaic effect.

1.5 General Description of the Photovoltaic effect

In 1954, the first silicon solar cells were invented, wherein, photo-excited charge carriers were separated by a built-in potential developed at p-n junction. The photovoltaic effect is the foundation of solar cells in which light is directly converted into electricity. A photovoltaic cell is a device that absorbs the photons of the sunlight and produces the free electron-hole pairs. The photovoltaic cells absorb those incident photons, which have higher band gap than the band gap of semiconducting layer. The photo-excited pairs are separated by built-in field and the separated charge carriers (electrons and holes) are transported to their respective electrode. These photo-carriers

circulate through an external load that supports a positive voltage and results in net delivery of electrical power to the outer circuit [G. L. Araujo et al. (1994); J. Bisquert (2018)]. This process of conversion of light to electricity is called the photovoltaic effect. The photovoltaic phenomenon in semiconductor-based solar cells and ferroelectric layer-based solar cells is differentiated by built-in-field. In conventional solar cells, the built-in field is due to p-n junction, while for ferroelectric solar cells this field is directly provided by polarization of ferroelectric layer. The bulk-photovoltaic phenomenon is described in Fig. 1.7 where E is the depolarization field opposite to the polarization direction. In ferroelectric based solar cells, the ferroelectric layer has two switchable polarization states (+P and –P), as depicted in Fig. 1.8(a). I-V curve depends on polarization state, as shown in Fig. 1.8(b).

The measurement of I-V curve in the dark and under light illumination is the main tool for the characterization of solar cells. The efficiency of a solar is based on how many incident light photons are converted into electrical energy, which we get in the form of current. So, the device efficiency (η) directly depends on current density (J_{sc}) in short circuit condition, open circuit voltage (V_{oc}), and the fill factor (FF) as given by the equations below:

$$\eta = \frac{V_{oc}\, J_{sc}\, FF}{P_{in}} 100\% \qquad \text{……...…… (1.3)}$$

Where P_{in} is incident light power = 1000 Wm^{-2} for A.M. 1.5G illumination (reference air mass 1.5 spectra as specified by ASTM) conditions and FF is defined as

$$FF = \frac{P_{max}}{V_{oc} J_{sc}} \qquad \text{…… (1.4)}$$

The position of parameters I_{sc}, V_{oc}, P_{max} in typical J-V plot is shown in Fig. 1.8(b). The FF is termed as a figure of merit of a solar cell, and it determines the position of maximum power point of the illuminated solar cell. J_{sc} is short-circuit current density of solar cells when voltage across the cell is zero. V_{oc} is the highest voltage generated by

the solar cell when no current flows. In conventional solar cells, V_{oc} depends on the band gap of the photo-absorbing layer but in ferroelectric V_{oc} depends on spontaneous polarization or photoconductivity or domain walls of the ferroelectric layer. The presence of a built-in electric field at domain walls causes charge separation and the above band gap voltage is due to an imbalance of polarization in the ferroelectric layer.

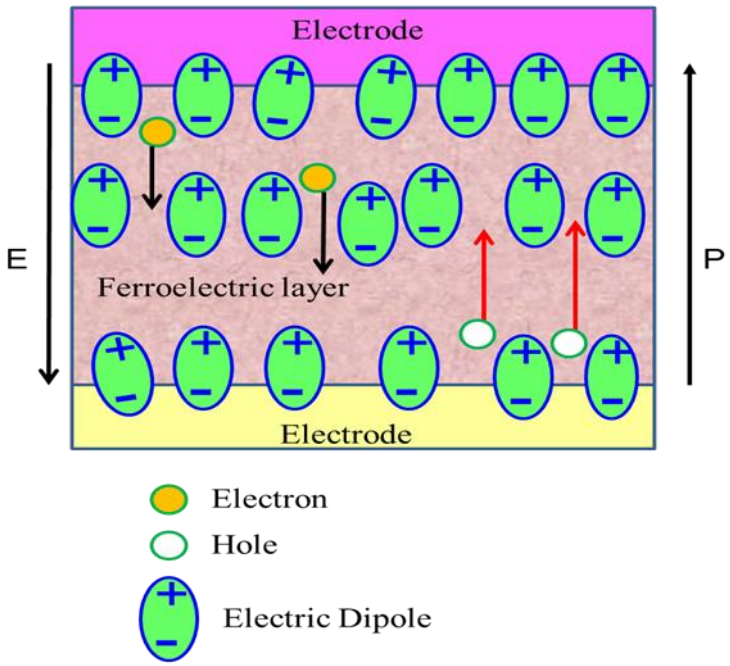

Figure 1.7 Schematic illustration of Bulk-photovoltaic effect in ferroelectric materials.

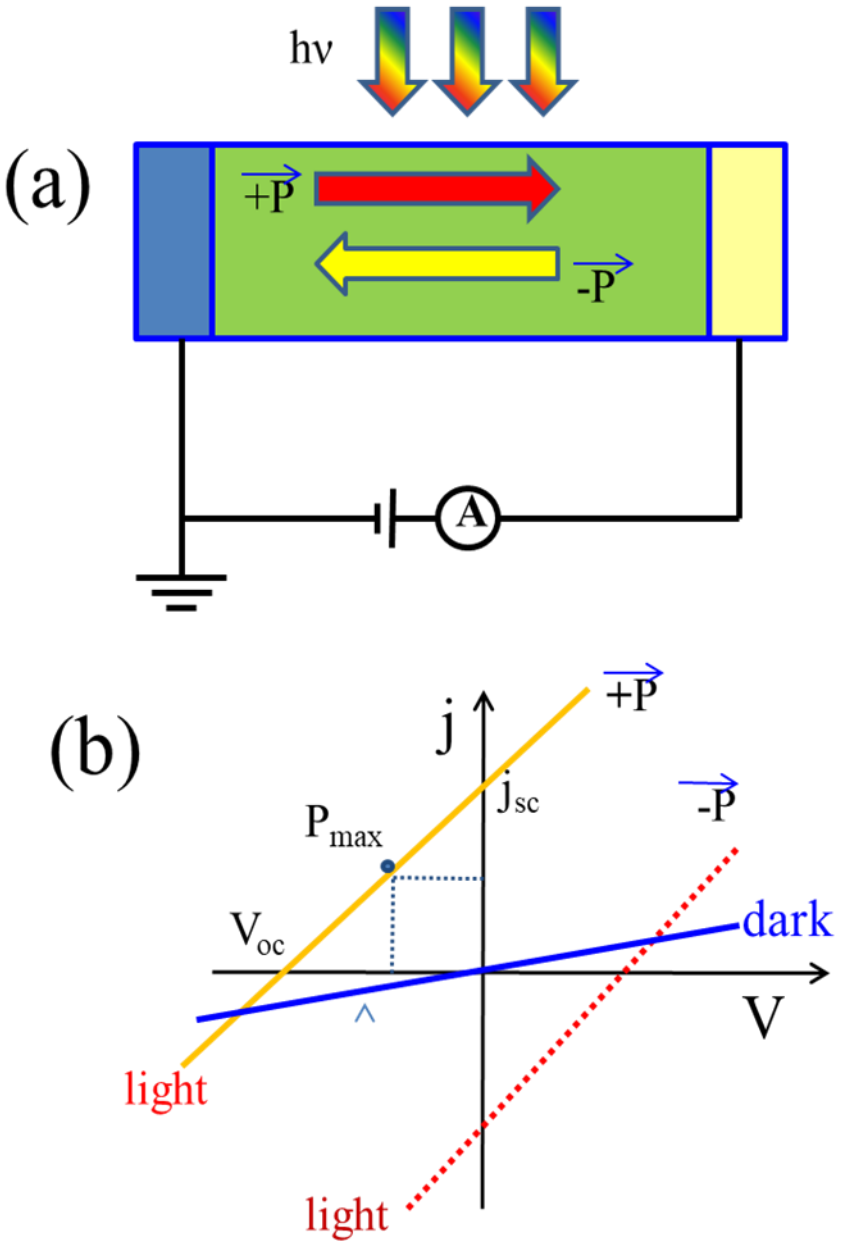

Figure 1.8 (a) Schematic diagram for bulk-photovoltaic mechanism and (b) typical curves for switchable bulk-photovoltaic effect.

1.6 Mechanism of Photo-voltaic effect in Ferroelectric materials

The light to electrical energy conversion in the photovoltaic process depends on the built-in field in the material which separates the photo-carriers. In silicon solar cells p-n junction is used for this purpose but in ferroelectric photovoltaic devices only single

layer is there and ferroelectric polarization plays the important role in charge separation. The physical origin of photo-voltaic (PV) effect in ferroelectric materials is still not well understood though it is explained by many theoretical models. According to P. S. Brody et al., the mechanism of anomalous PV effect can be explained in term of 'light-induced carriers screening an internal field within the bulk of spontaneously polarized grains". In this model, it is assumed that each grain has an individual grain photo-emf (electro motive force). These photo-voltages get added in series and the high ceramic photovoltage originates [P. S. Brody et al. (1975)]. The concept of this model is illustrated in Fig. 1.9. This mechanism is not able to explain complex cases of the polycrystalline ceramic microstructure adequately because it is very challenging to control the granular interface.

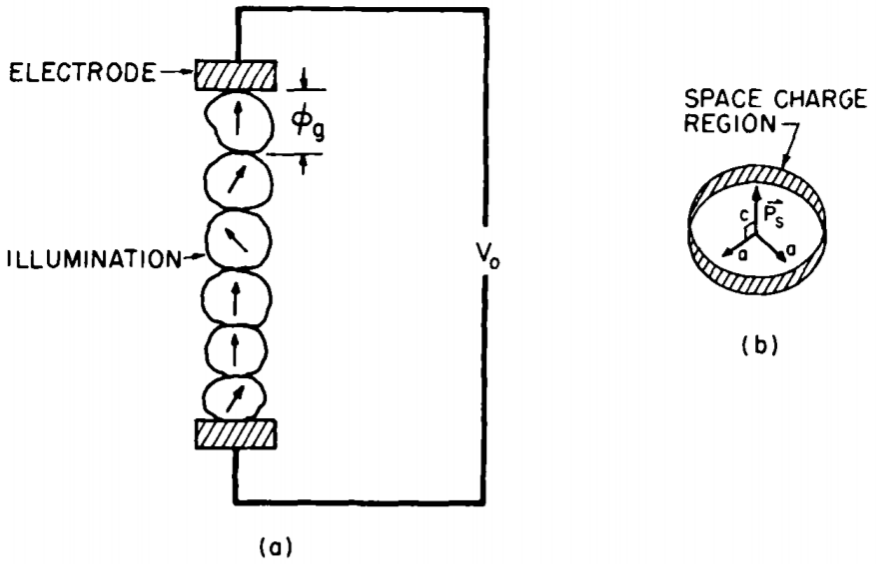

Figure 1.9 (a) Schematic demonstration of Photo-emf resulting across 'n' number of individual grains voltages addition to generate a net voltage V_o across edge electrodes. The arrows show the directions of spontaneous polarization (b) an individual grain illustrating area of space charge shielding the potential generated because of the polarization [P. S. Brody et al. (1975)].

1.6.1 Bulk-photovoltaic effect (BPVE)

Earlier reports on PV effect in ferroelectric materials have termed this as bulk photovoltaic effect (BPVE) with above band gap photovoltage. In BPV phenomena, the physical origin of PV effect is attributed to photo-carrier separation due to the lack of centre of symmetry. The BPVE has been explained by shift current mechanism where the driving force for charge separation is not a built-in electric field but the coherent evolution of electron and hole wave functions. According to the shift current model non-centrosymmetric crystals shows bulk photovoltaic current which consists ballistic and shift currents. The shift current contributes to the bulk photovoltaic effect. The shift current mechanism involves transfer of photo-carriers by the shift of the wave functions of charge carriers, and its amplitude is associated with the polarization of the electronic origin. The shift current model is based on quantum mechanical processes arising from the asymmetry in the electronic wave-function instead of the internal field [M. Nakamura et al. (2017)]. The total current in ferroelectric layer is given as

$$J = J_{sc} - \frac{V}{L}(\sigma_d + \sigma_{ph}) \qquad \text{..... (1.5)}$$

Where J_{sc} is the short-circuit shift current density, V is the photovoltage, L is the electrode distance, σ_d is dark conductivity and σ_{ph} is photoconductivity components. Thus, photocurrent and photovoltage show linear relationship with maximum fill factor of 0.25. Ferroelectric materials act as a current source as they have very low dark photo-conductivities [Y. Yuan et al. (2014); L. Z. Tan et al. (2016)]. The open circuit voltage (when J=0) is given as following:

$$J_{sc} = \frac{V_{oc}}{L}(\sigma_d + \sigma_{ph}) \qquad \text{..... (1.6)}$$

$$V_{oc} = \frac{J_{sc}}{(\sigma_d + \sigma_{ph})} L \qquad \text{.....(1.7)}$$

For thin samples, dark conductivity (σ_d) can be neglected

$$V_{oc} = \frac{J_{sc}}{(\sigma_{ph})} L \qquad \text{.....(1.8)}$$

The photo-induced electric field (E_p) due to the BPVE is given by

$$E_p = \frac{J_{sc}}{(\sigma_{ph})} \qquad \text{..... (1.9)}$$

The photoconductivity is given as,

$$\sigma_{ph} = e\, I_0\, \alpha\, \varphi\, (\hbar\omega)^{-1} (\mu\tau)_p$$

where 'e' is elementary charge, I_0 is incident light intensity, α is absorption coefficient, φ is quantum field, ħω is photon energy, μ is mobility of non-equilibrium carriers, τ is life time of non-equilibrium carriers [A. Zenkevich et al. (2014)]. In the case, photoconductivity become higher than the dark-conductivity of material, then, photovoltaic field in device shows the light intensity independent behaviour.

A. M. Glass et al have reported bulk photovoltaic effect with saturation voltage above 1000 V in $LiNbO_3$ crystals. They have proposed that the origin of PV effect in ferroelectric crystal can be attributed to bulk photovoltaic effect which results from the asymmetry of the lattice [A. M. Glass (1974)]. BPV effect has two characteristic features; the photocurrent and photovoltage depend on the polarization of light. The direction of photocurrent can be changed by changing the sign of the circular light polarization. Photovoltage value can be exceeding the band gap value of the material. BPVE is observed in non-centrosymmetric (piezoelectric and ferroelectric) crystals. This effect was experimentally reported in tellurium crystals [B. I. Sturman and V. M. Fridkin (1992)]. According to Fredkin et al, the physical origin of BPVE can be related to excitation in a crystal of the non-thermalized electrons or holes [V. M. Fridkin (2001)]. Fig.1.10 (a) depicts the intrinsic excitation in a centrosymmetric crystal. The electron distribution in the band is symmetric and there is no current.

Fig.1.10 (b) shows the excitation in a non-centrosymmetric crystal where asymmetric momentum distribution for electron persists. The photo-excited non-thermalized electrons loss energy and move down to the band bottom. This mechanism results in the shift 'l_0' and thus affects the mobility of photoelectrons, and thus PV effect is observed. T. Choi et al. have demonstrated switchable ferroelectric diode effect and photovoltaic effect in $BiFeO_3$ single crystal [T. Choi et al. (2009)].

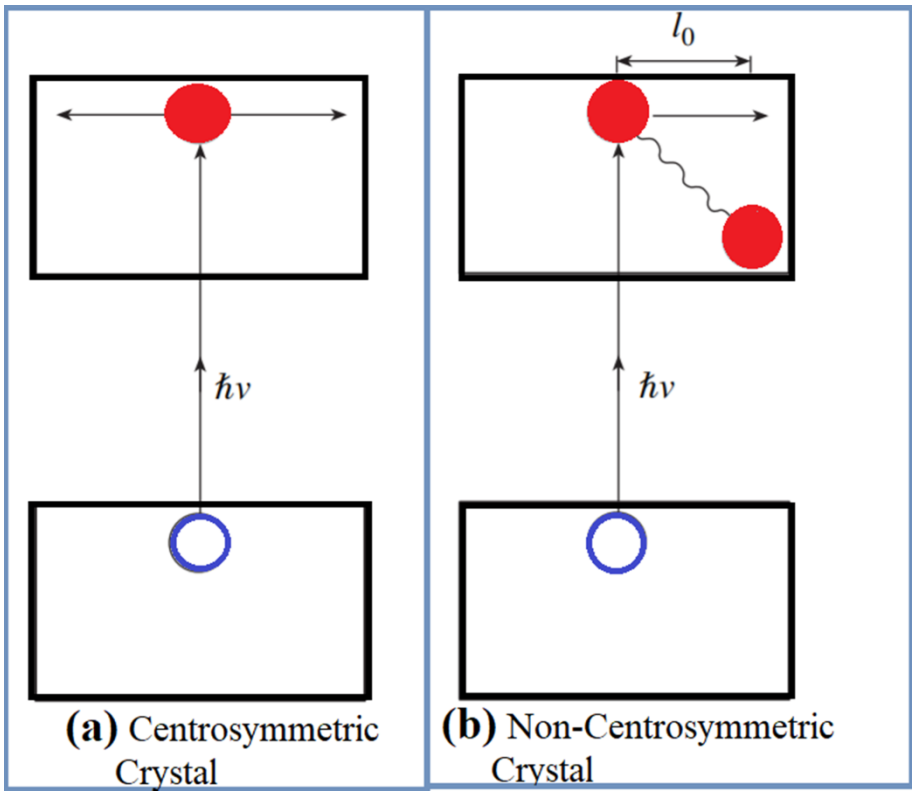

Figure 1.10 (a) A schematic representation of symmetric distribution of nonequilibrium carriers in a centrosymmetric crystal; (b) Asymmetric distribution of nonthermalized carriers in a non-centrosymmetric crystal [after V. M. Fridkin et al. (2001)].

1.6.2 Depolarization field model

The first concept of depolarization field in the thin ferroelectric film has been coined by R. R. Mehta et al. [R. R. Mehta et al. (1973)]. In this model, depolarization field is assumed as a driving force for separation of photo-carriers. This field arises from the incomplete screening of charges due to polarization. The polarization of any

dielectric medium is defined as the dipole moment per unit volume. The dielectric dipole is a system having a positive and negative charge. Polarization of dielectric generates a macroscopic electric field which is sum of applied field and depolarization field. The depolarization field is due to the uniform polarization of dielectric material. The direction of depolarization field is opposite to applied electric field as illustrated in Fig. 1.11. The depolarization field is due to the polarization charges lying at the outer surfaces of the material [C. Kittel (2012)]. Ferroelectric thin films can generate polarization charges on the surface when any field is applied. These charges induce an electric field inside the layer. In capacitor form, the ferroelectric layer is sandwiched between metal or semiconducting electrodes, and the outer surface charges can be screened but practically screening is incomplete, and it produces an electric field inside layer termed as depolarization field.

R. R. Mehta and co-workers have proposed a mechanism to explain the depolarization phenomena in thin ferroelectric films [R. R. Mehta et al. (1973)]. They have considered a ferroelectric capacitor sandwiched between two metal electrodes as shown in Fig. 1.12. The ferroelectric layer is poled with polarization P. Due to this polarization, "± q e" charges generate in the metal electrodes. R. R. Mehta et al. have proposed that metal-ferroelectric-metal capacitor have depolarization field when the compensation charge is distributed away from the ferroelectric-metal electrode interface. They have shown that the work function differences of the electrodes and trapped interface charges give an internal bias which can be observed by induced polarization [R. R. Mehta et al. (1973)]. I.P. Batra et al. have reported that polarization in a thin ferroelectric film sandwiched between semiconducting contacts is not completely neutralized by external charges. These remaining charges create a field opposite to the polarization, which is called depolarization field. Fig. 1.13 illustrates

how the fields are distributed in ferroelectric film [I. P. Batra et al. (1973)]. The remaining charges spread over near the interface and create a charged region. When field from ferroelectric film penetrates over this region into the contacts, a band bending occurs near electrode due to potential drop. This band bending (V_b) generates the depolarization field in the ferroelectric film. The depolarization field is thickness dependent and shows large value for thin layers. Due to a biasing potential V_a, the Fermi levels E_f into semiconducting electrodes are raised by qV_a.

For a uniformly polarized ferroelectric, the compensation charges accumulate near the ferroelectric/electrode interfaces, and cause bending conduction band (E_c) and valence bands (E_v) in the semiconducting electrodes. The band bending potential in electrode is given by

$$V_b = \frac{kT}{q} ln\left(\frac{2\pi\rho_0^2}{\varepsilon n_i(T) kT}\right) \quad \ldots\ldots\ldots\ldots\ldots\ldots\ldots\ldots (1.10)$$

Where k is Boltzmann constant, T is temperature, n_i is the intrinsic carrier density, ρ_0 is the total charge per unit area in electrode and q is the electronic charge [I. P. Batra et al. (1973)]. The magnitude of depolarization field due to spontaneous alignment of the electric dipoles is

$$E_{d=} = -\frac{P}{\varepsilon_0 \varepsilon_{ferro}} \quad \ldots\ldots\ldots\ldots\ldots\ldots\ldots\ldots\ldots\ldots (1.11)$$

Where P is the ferroelectric polarization ε_0 is dielectric constant of vacuum and ε_{ferro} is the linear dielectric constant of ferroelectric [C. T. Black (1997)].

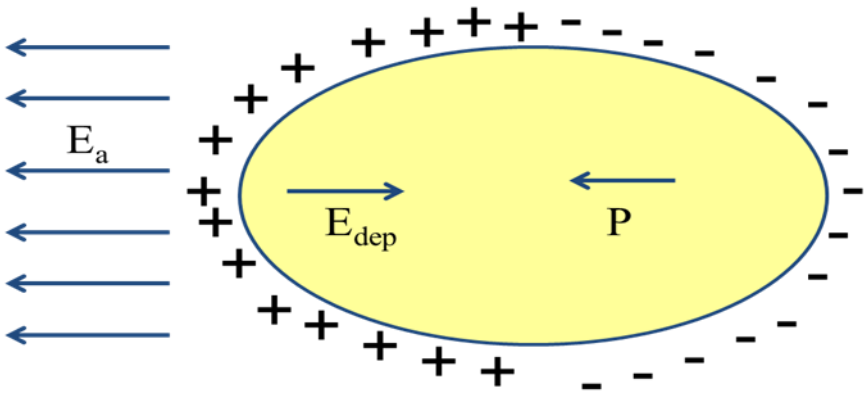

Figure 1.11 Direction of depolarization field inside the ferroelectric

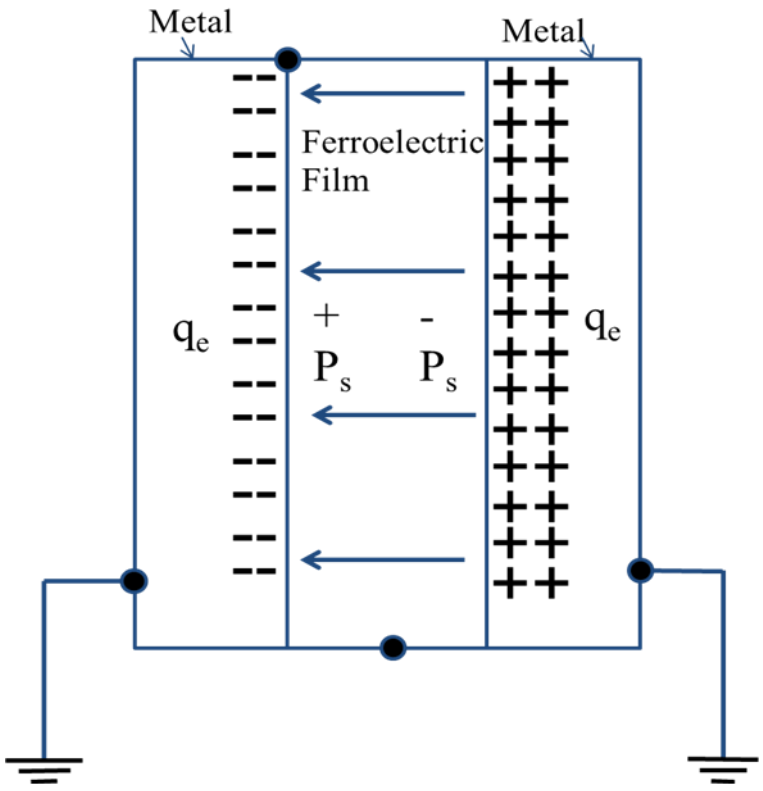

Figure 1.12 Thin-film ferroelectric sandwiched capacitor: a poled ferroelectric layer sandwiched between two metal electrodes (RR Mehta et al. (1973)].

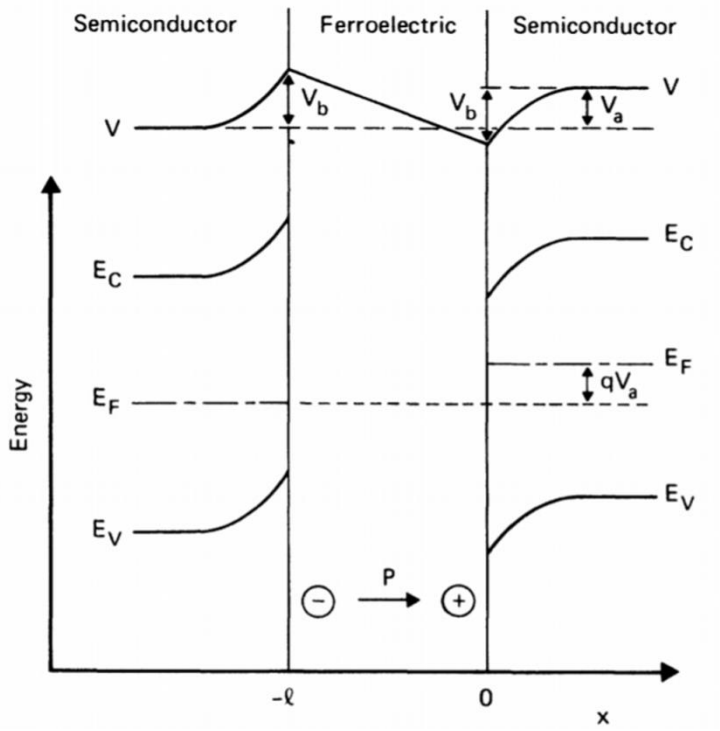

Figure 1.13 Distribution of potential V in a ferroelectric semiconductor configuration [I. P. Batra et al. (1973)].

M. Dawber and co-workers have reported that depolarization field depends on type of electrode and affects the charge compensation at the ferroelectric-electrode interface and correlated the depolarization field (E_d) with coercive field (E_c) in following way; $E_{meas.} = E_c - E_d$ where $E_d = (8\pi P_s \lambda)/(\varepsilon_e d)$, where ε_e is the dielectric constant of the electrode, d is the thickness of ferroelectric layer, P_s is spontaneous polarization and λ is screening length [M. Dawber et al. (2003)].

D. J. Kim et al. have experimentally determined the depolarization field (E_d) in $SrRuO_3/BaTiO_3/SrRuO_3$ capacitor using following equation

$$E_d = -\frac{P}{\varepsilon_0 \varepsilon_F}\left(\frac{2\varepsilon_F/d}{2\varepsilon_F/d + \varepsilon_e/\lambda}\right) \qquad \ldots\ldots\ldots\ldots\ldots\ldots\ldots (1.12)$$

Where ε_e and ε_F are the relative dielectric constant of the electrode and ferroelectric layer respectively, d is the film thickness and P is the polarization. The depolarization field E_d for $BaTiO_3$ is found around 300 kV/cm [D. J. Kim et al. (2005)]. The

depolarization field is the onset of domain-wall flow and it should be equal to activation field E_a in order to move the domain walls [D. Zhao et al. (2019)].

M. Qin and co-workers have used depolarization field model to explain the thickness dependent photocurrent in ferroelectric films and a relation between internal electric field and photocurrent has been analyzed in $(Pb_{0.97}, La_{0.03})(Zr_{0.52}, Ti_{0.48})O_3$ thin film based capacitor [M. Qin et al. (2007); M. Qin et al. (2009)]. B. Chen et al. have used depolarization field model to explain the origin of photovoltaic effect in $BiFeO_3$ ferroelectric film (ITO/BFO/Pt capacitor). The electric field in ferroelectric film capacitor can be defined as $E= E_{bi}+E_d$, where E_{bi} is the built-in field and E_d is the depolarization field. They have calculated that a higher depolarization field help to separate the photo carriers easily [B. Chen et al. (2011)]. R. Guo and co-workers have studied ferroelectric photovoltaic effect in epitaxial $BiFeO_3$ film (100 nm). The $BiFeO_3/La_{0.7}Sr_{0.3}MnO_3$ based capacitor have depolarization field which separate and transport the photo-carriers before they recombine [R. Guo et al. (2013)].

H. Han et al. concluded that h-$RFeO_3$ films have large ferroelectric polarization which reduces a rapid recombination rate of photo-carriers and the device efficiency depends on polarization of h-$RFeO_3$ films. Device having ITO/h-$RFeO_3$/Pt heterostructure shows switchable photovoltaic effect. The photocurrent of the h-$TmFeO_3$ is more than the h-$LuFeO_3$ and it is correlated to their remanent polarization (P_r) value. The P_r of h-$TmFeO_3$ is 1.8 times higher than that of h-LuFeO3. The higher P_r separates photo-carriers more effectively [H. Han et al. (2018)]. A. B. Swain and co-workers have shown that depolarization field dominates the photovoltaic response beyond coercive field as compared to Schottky effect in $0.5Ba(Zr_{0.2}Ti_{0.8})O_3$-$0.5(Ba_{0.7}Ca_{0.3})TiO_3$ (BZT-BCT). They have calculated the depolarization field E_d for BZT-BCT at 3V and found E_d = 0.088 MV/m and E_d = 2.9MV/m at 8V poling. Fig.1.14

(a) is showing the effect of poling voltage and Fig.1.14(c) illustrates the schematic of energy band diagram at different poling voltages [A. B. Swain et al. (2019)].

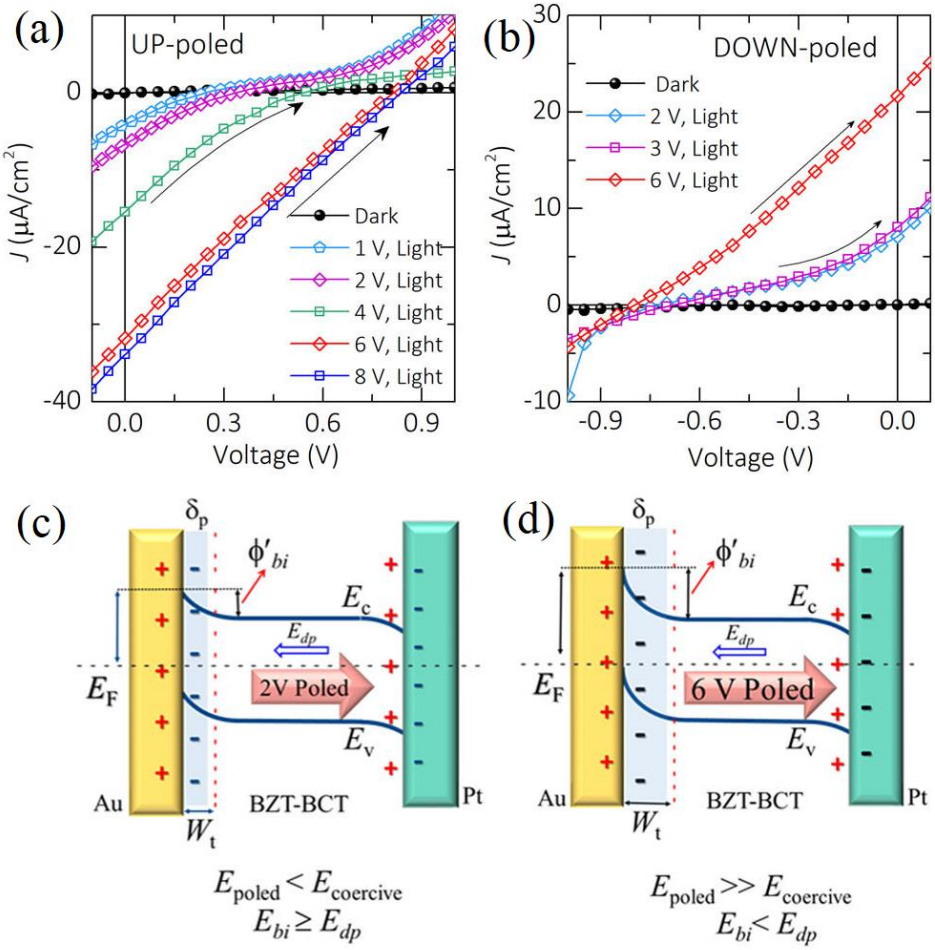

Figure 1.14 current density-voltage curves for (a) Upward-poling and (b) Downward-poling condition of the BZT-BCT film measured in dark and under light conditions. Graphic presentation of energy band diagram illustrating the deviation of the barrier field for (c) poled with $E_{poled} < E_{coercive}$, and (d) poled with $E_{poled} > E_{coercive}$ states of the Au/BZT-BCT/Pt film. Here, W_t is the depletion widths at the top, W_b is bottom electrode/film interfaces and δ_P is the polarization charge due to poling. [A B Swain et al. (2019)].

1.6.3 Domain wall effect

The bulk-photovoltaic effect mechanism is applicable only for wide-band gap semiconductors (E_g > 2.5 eV), so, photovoltaic effect at nanoscale cannot be explained in term of inherent non-centrosymmetry in polar material. So, another theoretical model was proposed by S. Y. Yang et al. (2009) to explain the physical origin of BPVE in polar materials which is based on ferroelectric domain wall model. They have reported that photocarriers generation and separation process occurs at nanometre-scale ferroelectric domain walls. In domain wall based mechanism, the photo-excited charge carriers are separated by potential step developed at an individual ferroelectric domain wall. According to the model proposed by Yang et al., the high photovoltage in $BiFeO_3$ (BFO) epitaxial films get originated from the domain walls of the ferroelectric material. The domain wall acts in a similar way as p-n junction and the operational principle of both mechanisms are compared as depicted in Fig.1.15. In ferroelectric solar cells the band bending occurs across the domain walls [H. Huang (2010)]. Fig. 1.16 illustrates the domain wall model and photovoltaic mechanism according to it [S. Y. Yang et al. (2009)]. The component of the polarization perpendicular to domain wall of BFO consist the built-in potential steps and associated charge density forms an electric dipole. The electric dipoles generate an electric field within the domain wall and potential step. Under light illumination, the BFO domain walls separate the photocarriers around walls as shown in Fig 1.16 (d). The combined local electric field due to domain walls results in a net high photovoltaic voltage across the entire sample [S. Y. Yang et al. (2009); J. Seidel et al. (2009)]. According to domain wall model S. Y. Yang and co-workers have shown that above band gap open circuit voltage was only observed when the electrodes were parallel to the domain walls in BFO. When electrode

configuration was parallel to the domain walls no V_{oc} was observed as illustrated in Fig 1.17.

W. Ji et al. have reported PV responses in parallel to the ferroelectric polarization direction**.** This observation suggests that BPVE is also noteworthy even in materials with domain walls [W. Ji et al. (2010)]. S. M. Young et al. have theoretically computed BPV effect in BFO and found that bulk photovoltaic effect will somewhat terminate domain-wall driven carrier separation [S. M. Young et al. (2012)]. A. Bhatnagar and co-workers have further reported the photovoltaic effect in BFO films. They achieved very high V_{oc}~ 50V in BFO films by controlling the conductivity of domain walls [A. Bhatnagar et al. (2013)].

S. Y. Yang et al. have reported V_{oc} in BFO only when electrodes were parallel to domain walls whereas A. Bhatnagar et al. have achieved higher V_{oc} in both parallel and perpendicular directions as shown in Fig 1.18(d) [S. Y. Yang et al. (2009)]. They have confirmed that abnormal photovoltaic effect in $BiFeO_3$ film is because of Bulk-Photovoltaic effect. To explain the PV effect origin in BFO, two resistance model has been used as shown in Fig 1.18(g) and (h). In the perpendicular to domain wall (PPDW) geometry, the equivalent circuit is a parallel circuit and total conductivity $\sigma_{total} = (\sigma_{bulk} + \sigma_{DW})$. In parallel to domain wall (PLDW) geometry, the equivalent circuit is the series circuit and total conductivity $(\sigma_{total})^{-1} = (\sigma_{bulk})^{-1} + (\sigma_{DW})^{-1}$. According to this model, effective resistance is lower when DWs are perpendicular to the electrodes thus V_{oc} should be lower [A. Bhatnagar et al. (2013)].

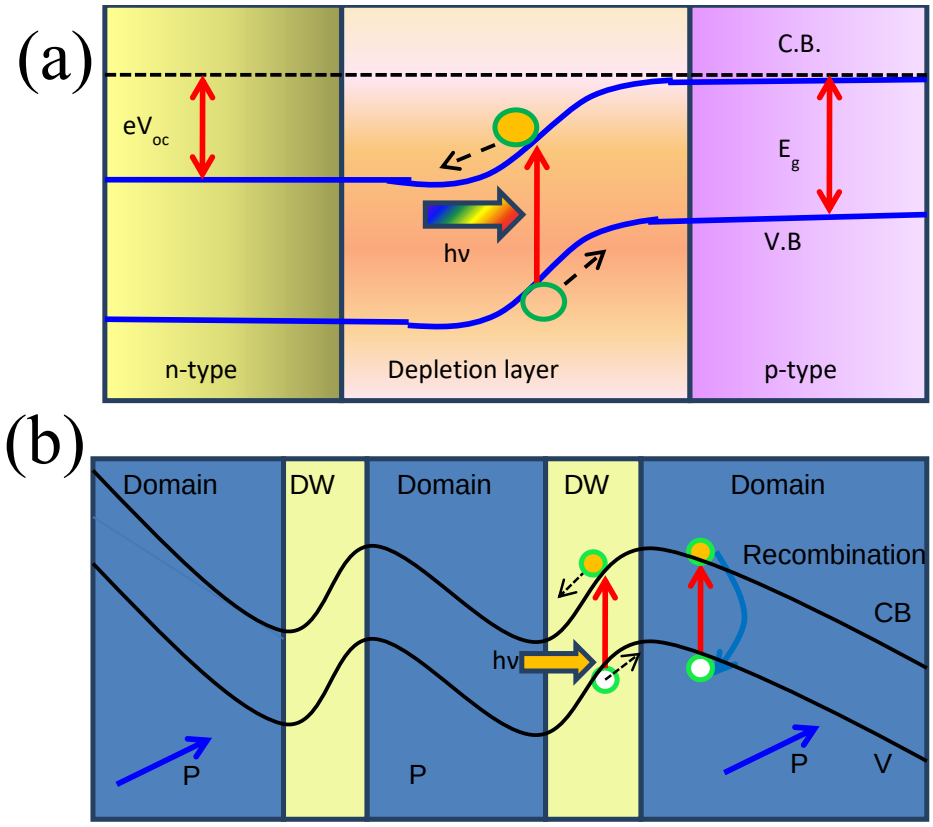

Figure 1.15 Mechanism of photovoltaic effect in (a) conventional p-n junction solar cell and (b) Ferroelectric photovoltaic cell, in the ferroelectric domain, band bending occurs across the domain wall (DW). Arrows represent the directions of electric polarization (P) [H. Huang (2010)].

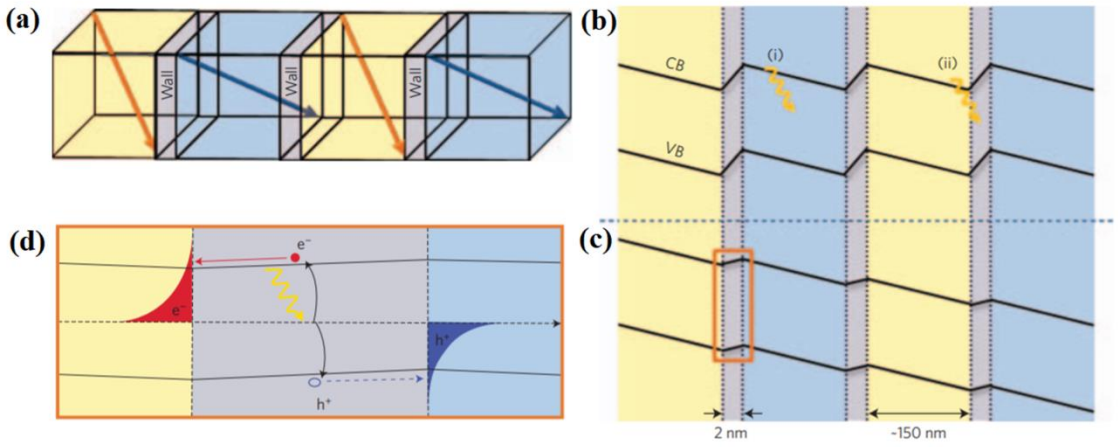

Figure 1.16 Schematic illustration of band structure in dark and light (a) four domains (three domain walls) in an order array of 71° domain walls. (b) Corresponding band diagram showing the VB and CB across these domains and domain walls in the dark condition. In Fig.(b) section (i) shows a photon hitting in the bulk of a domain and section (ii) a photon hitting at a domain wall. (c) Progression of band structure upon illumination of the domain wall array. (d) Comprehensive representation of the build-up of photo excited charges at a domain wall [S. Y. Yang et al. (2009)].

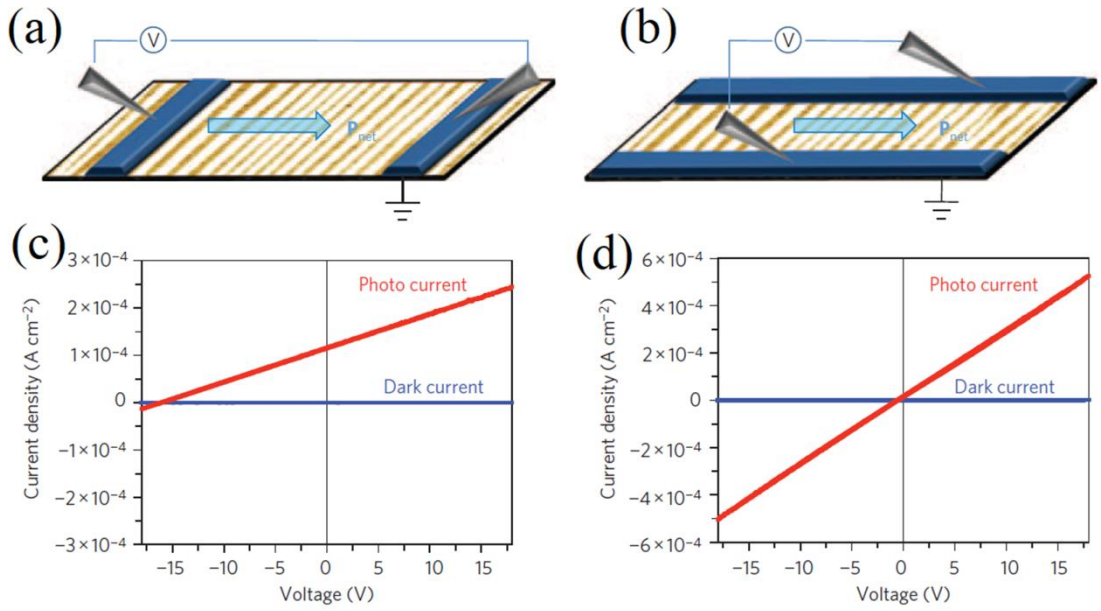

Figure 1.17 Schematics of the (a) perpendicular domain wall (b) the parallel domain wall device geometries and (c), (d) Corresponding I–V measurements respectively [S. Y. Yang et al. (2009)].

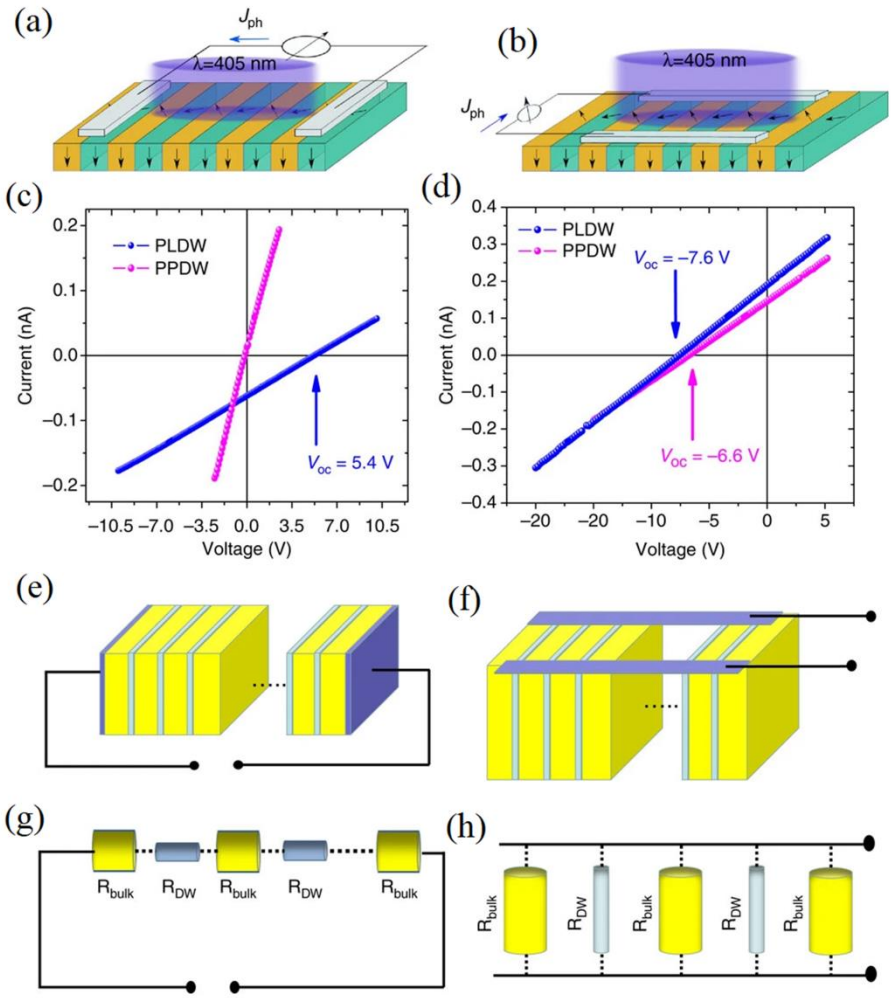

Figure 1.18 Schematic figure depicting majority 71° domains (not to scale) and typical measurement geometries in which the electrodes are running: (**a**) parallel to domain wall (PLDW) and (**b**) perpendicular to domain wall (PPDW), respectively. I-V characteristics under illumination with monochromatic light ($h\upsilon$=3.05 eV) of BFO thin films comprising (**c**) 109° and (**d**) 71° periodic stripe domains. A schematic showing the periodic arrangement of domains and domain wall in BFO thin films for the (e) PLDW and (f) PPDW geometry with respect to the DW. An equivalent circuit considering that the domain bulk and DW have different resistances, R_{bulk} and R_{DW}, is shown for both the geometries in (g) PLDW and (h) PPDW [A. Bhatnagar et al. (2013)].

1.6.4 Schottky diode model

It is well established that, the built-in-field (E_{bi}) in the depletion region bring forth the driving force for charge separation for photogenerated charge carriers. The Schottky junction is formed at ferroelectric and metal interface with a similar region. Electrode-ferroelectric interface creates a barrier which is called Schottky barrier and it can be ideally determined by the difference of metal electrode work function and ferroelectric film's electron affinity. In early reports, the effect of Schottky junction was ignored for ferroelectric devices as they show very high photovoltage. The photovoltage due to Schottky junction effect depends on band gap of material and is calculated by Schottky barrier height difference at both interfaces. The ferroelectric photovoltaic devices that have same type of the electrodes show no contribution in net built-in-potential as Schottky barrier height difference become zero.

L. Fang et al have reported that PV effect in Pt/$BiFeO_3$/$La_{0.7}Sr_{0.3}MnO_3$ is mainly due to the Schottky barrier modulation by ferroelectric polarization [L. Fang et al. (2014)]. C. Wang et al. have also proposed the Schottky model-based explanation of switchable photovoltaic effect in $BiFeO_3$ as illustrated in Fig.1.19. The Fermi-level of $BiFeO_3$ (BFO) is higher than that of $SrRuO_3$ (SRO) (as one electrode) and Pt (as the other electrode), so, few electrons in the BFO should move into SRO and Pt. When some electrons leave BFO, few positive charges are created there and form a positively charged region at BFO/electrode interfaces. The electrically charged region termed as depolarization region gives a built-in-field created in opposite direction. This built-in-field coming from the Schottky interface barriers (E_{bi}) promote the photo-carriers separation [C. Wang et al. (2011)]. D. Cao et al. have analyzed the photovoltaic effect in Pt/$Pb(Zr_{0.2}Ti_{0.8})O_3$/Pt capacitor and found that top and bottom Pt/film interfaces form Schottky diodes in series as shown in Fig.1.20. The net built-in-electric field produced

from the Schottky barrier is defined as $E_{bi} = E_{bi\text{-}bottom} - E_{bi\text{-}top}$, where $E_{bi\text{-}bottom}$ and $E_{bi\text{-}top}$ are the Schottky barriers from bottom and top Pt/PZT interface respectively [D. Cao et al. (2010)]. The formation of Schottky barriers for Pt/Pb($Zr_{0.2}Ti_{0.8}$)O_3/Pt film interfaces is explained in Fig.1.20.

H. Han et al. have used combined approach of depolarization field and Schottky model to explain the switchable photovoltaic effect in hexagonal $RFeO_3$ films. A schematic energy band diagram is used to explain the combined effect of depolarization field and Schottky barrier effect on the origin of PV effect in h-$LuFeO_3$ films as shown in Fig.1.21. The Schottky barrier height at Pt/h-LFO junction is given as

$$\varphi_{Pt/LFO} = \varphi_{Pt} - \varphi_{LFO} = 5.30 \text{ eV} - 4.60 \text{ eV} = +0.70 \text{ eV}$$

The Ohmic anti-barrier depth at ITO/h-LFO is

$$\varphi_{ITO/LFO} = \varphi_{ITO} - \varphi_{LFO} = 4.40 \text{ eV} - 4.60 \text{ eV} = -0.20 \text{ eV}$$

The barrier-height difference provides the net built-in potential

$$\Delta E = \varphi_{Pt/LFO} - \varphi_{ITO/LFO} = 0.70 \text{ eV} - (0.20 \text{ eV}) = +0.90 \text{ eV}$$

In upward poling condition, the higher photocurrent is observed because direction of E_d is parallel to $E_{net} = E_{bi} + E_{dp}$ and under downward poling the directions are opposite so net built-in field reduced [H. Han et al. (2018)].

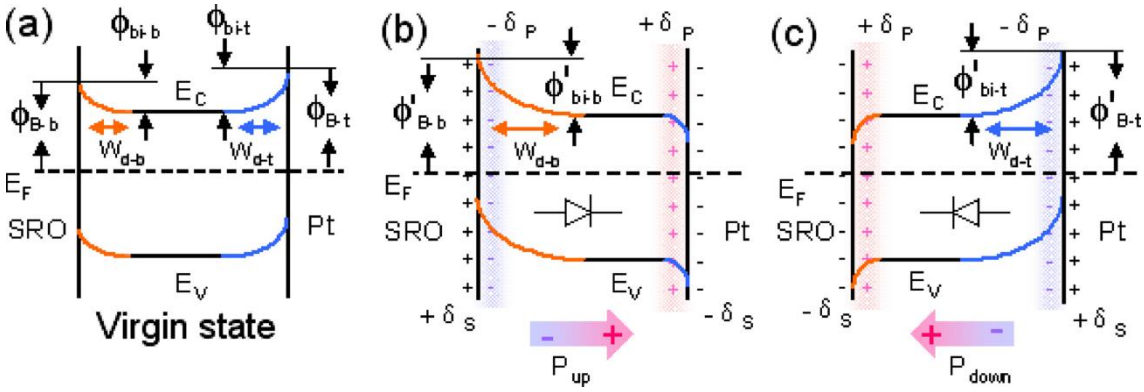

Figure 1.19 A simplified illustration of energy band diagrams presenting the variations in Schottky barriers from back-to-back diodes at virgin (a) to a forward diode at polarized up (b) and a reverse diode at polarized down (c) [C Wang et al. (2011)].

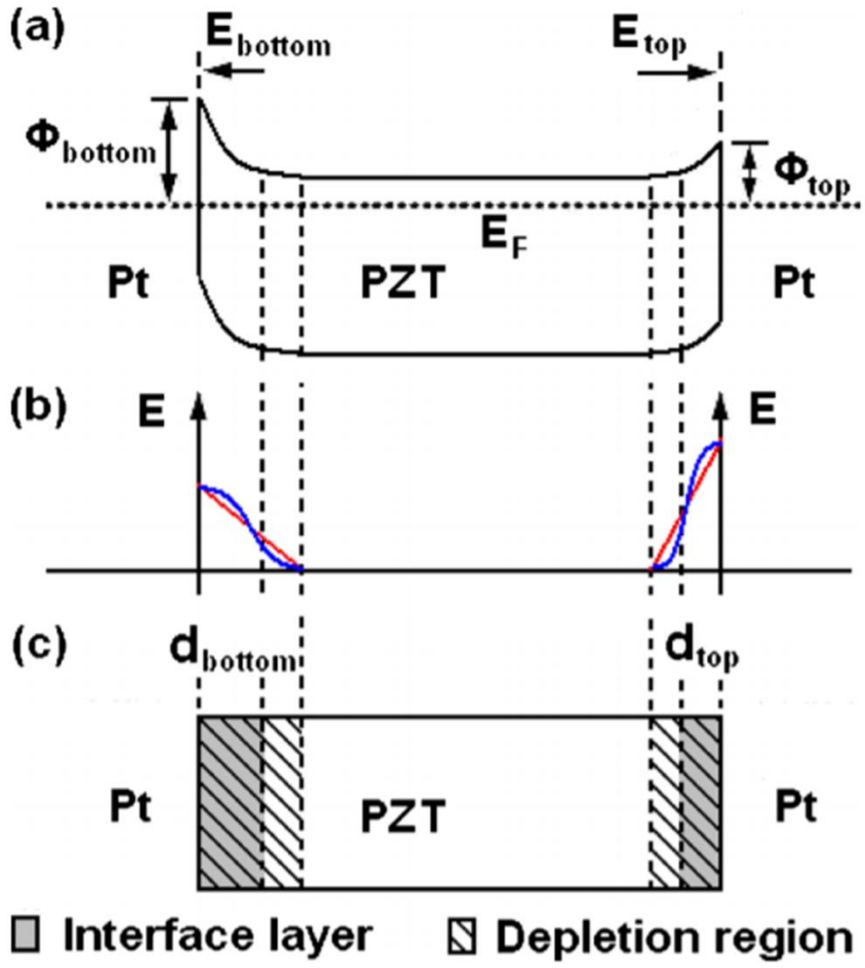

Figure 1.20 schematic representations of (a) asymmetric Schottky barriers, (b) built-in electric field distributions: red or blue line specifies the electric field with or without the interface layer and (c) top and bottom interface layers in Pt/PZT/Pt capacitor. [(D. Cao et al. (2010)]

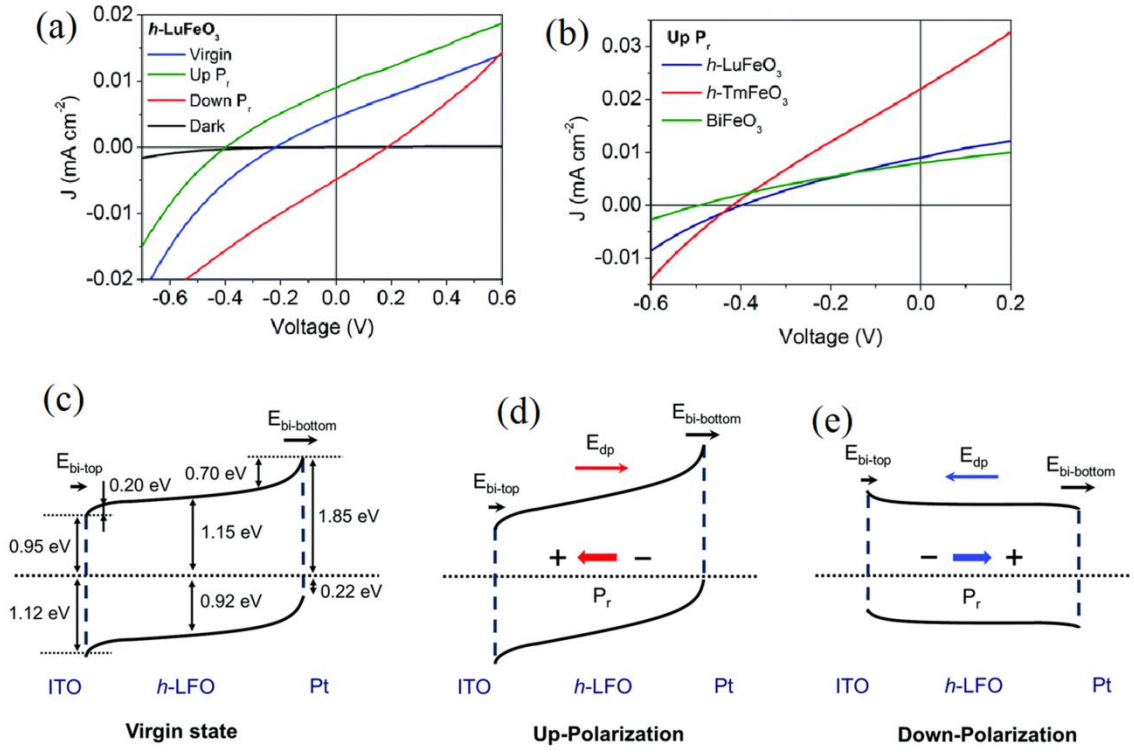

Figure 1.21 Current density (J)–voltage (V) curve of (a) ITO/h-LFO/Pt (b) ITO/h-TFO/Pt device compared with ITO/h-LFO/Pt and ITO/BFO/SRO devices after upward poling. Modulated energy band diagrams of ITO/h-LFO/Pt (c) the virgin state (d) up-polarization state (e) down-polarization state [H. Han et al. (2018)].

1.7 Strategies to improve PV efficiency in ferroelectric oxide solar cells

The photovoltaic device efficiency depends on various factors such as band gap of photo active material, its light absorption efficiency, excitation dissociation and charge collection efficiency. The general device structure of solar cell is composed of photo-absorbing layer and two charge extracting electrode. The solar energy conversion is based on the extraction of non-equilibrium charge carriers, before their recombination, so that the charge collection efficiency sufficiently increases. To achieve large charge collection efficiency, the effective separation of the electron hole pair is required. The electron-hole pair is formed by the excitation dipole at the area of the photo-generation process. So, proper excitation dissociation process (electron hole separation) is the first step to increase the charge collection efficiency. Next step is transportation of separated holes and electrons to their respective electrodes. In ferroelectric materials based solar cells the central layer consists of only single material which act as photo-absorbing layer and also provide potential for separation and transportation of electrons and holes. In organic and DSC solar cells, central layer acts as photo-absorbing layer while for charge transportation, electron and hole transport layers are inserted between electrode and photoactive layer.

1.7.1 Optical band gap engineering of ferroelectric layer

The photocurrent resulting from the solar cells depend on the amount of light absorbed by photoactive layer and light absorption efficiency of material is directly proportional to its optical band gap. Till now, low photocurrent is reported in solar cells using ferroelectric materials as active layer because of their wide band gap. Several doping strategies are adopted to engineer the band gap of ferroelectric materials. The ferroelectric materials like $PbTiO_3$, $BaTiO_3$ and $KNbO_3$ have a band gap more than 3.0 eV. It is extremely enviable to decrease the band gap of ferroelectric materials to get

high photocurrent. The wide band gap ferroelectric materials can absorb only ultraviolet light which is 3.5% of the solar radiation intensity. The visible light comprises 40% of the solar radiation and therefore, the efficient materials for solar cells applications require a band gap near 1.7 eV for high light absorption. Widely investigated ferroelectric $BiFeO_3$ has band gap around 2.2 eV to 2.7eV. Thus, it can absorb light up to only 560 nm. Recent theoretical and experimental studies have reported that the band gap of ABO_3-type perovskite ferroelectric materials can be altered and tuned by transition metal substitution at B-site. To get suitable ferroelectric photovoltaic solar cell materials, various schemes were applied to decrease the band gap of ferroelectric materials so that they absorb incident light photons over a broad spectral range.

The transition elements doping can be effectively used to decrease the band gap of ABO_3 type perovskites. R. Inove et al. have investigated Mn doped $BaTiO_3$ single crystals and reported drastic increase in photocurrent as shown in Fig 1.22. $BaTiO_3$ single crystal shows J_{sc} ~ 36 pA/cm^2 which increased 285 pA/cm^2 when doped with 0.25% Mn under the $h\nu < 2$ eV light irradiation. Fig 1.22(d) shows the defect states in the electronic band structure for Mn doped $BaTiO_3$ single crystals. Due to Mn doping absorption coefficient of BTO is increased and two Mn-d related defect states are formed at 1.8 eV and 1.2 eV with respect to valence band maximum. The increase in photocurrent is due to electron excitation from O-2p valence band to the Mn- e_g defect level followed by hole injection [R. Inoue et al. (2013)]. W. S. Choi et al. have reported reduced band gap for $Bi_4Ti_3O_{12}$ ferroelectric material from 3.55 eV to 2.65 eV by site-specific alloying of $LaCoO_3$. The increased photocurrent in $LaCoO_3$ alloyed $Bi_4Ti_3O_{12}$ confirms the band reduction as shown in Fig. 1.23 [W. S. Choi et al. (2012)].

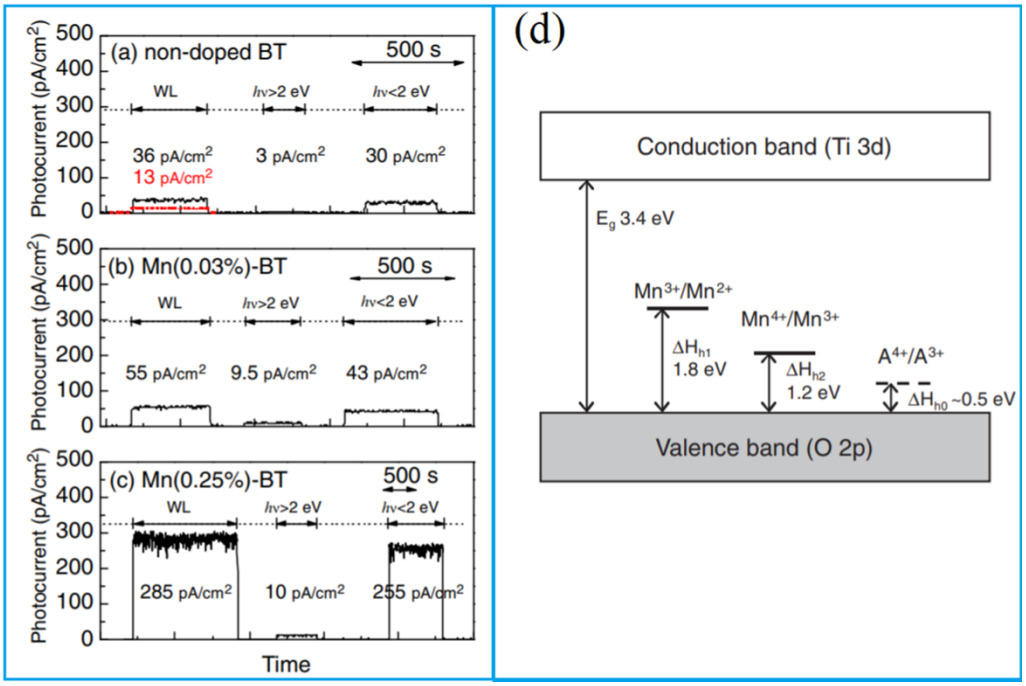

Figure 1.22 Photocurrent properties for the (a) BT, (b) Mn(0.03%)-BT, and (c) Mn(0.25%)-BT crystals. (d) Defect states in the electronic band structure of BT and Mn-BT (A = Al, Fe etc.) [R. Inoue et al. (2013)].

G. Zhang et al. have proposed that reduced oxygen coordination could offer a strategy to achieve low band gap ferroelectric materials. They have reported a new multiferroic $KBiFe_2O_5$ material which shows much lower E_g ~ 1.6 eV and J_{sc} ~ 15 $\mu A/cm^2$ and V_{oc} ~ 9.1V as shown in Fig. 1.24 [G. Zhang et al. (2013)]. R. Nechache et al. have applied cationic ordering approach to reduce the band gap of Bi_2FeCrO_6 and achieve band gap E_g ~ 1.4 eV by tailoring the Fe/Cr cation ordering and the ordered domain size. The Bi_2FeCrO_6 multilayer device shows J_{sc} ~ 20.6 mA/cm^2 with 8.1% device efficiency, so it can be concluded that optical band gap is dominant factor to increase the device efficiency. H. Matsuo et al have adopted 'gap-state' engineering approach to produce photo-ferroelectrics in which defect states within the band gap act as a platform for photo-generation. Half of these defect states are filled with electrons. Empty states receive electrons from the valence band and filled states supply them to conduction band, thus generating electron-hole pairs. Fig 1.25 shows the schematic

band structure of the transition element doped $BiFeO_3$. Cr, Mn and Co produces the gap states. Fig 1.25 compares the J-V properties of undoped and Mn doped $BiFeO_3$. The Mn-doped BFO shows high photocurrent J_y ~ -15μA/cm^2 than that of BFO film (~ J_y ~ 1.3μA/cm^2) [H. Matsua et al. (2017)].

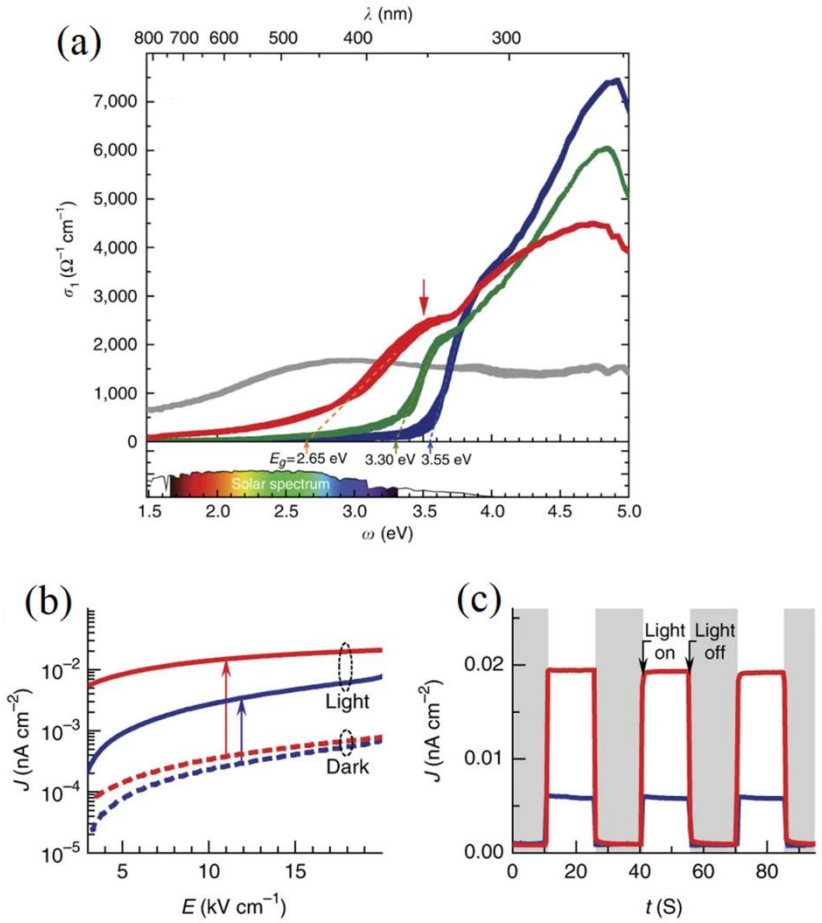

Figure 1.23 (a) Optical conductivity of BiT (blue), $1Bi_4Ti_3O_{12}$–$1LaCoO_3$ (1B2L) (red) and LCO (grey) confirms an orderly and considerable decline in bandgap values on site-specific substitution of BiT with La and Co (b) Photo-current density (J)-Electric field (E) curves (c) Photoresponse J-t curve from BiT (blue) and 1B2L (red) thin films (c) J recorded from BiT (blue) and 1B2L (red) thin films by switching on and off the solar simulator at 20 kVcm^{-1}[W. S. Choi et al. (2012)].

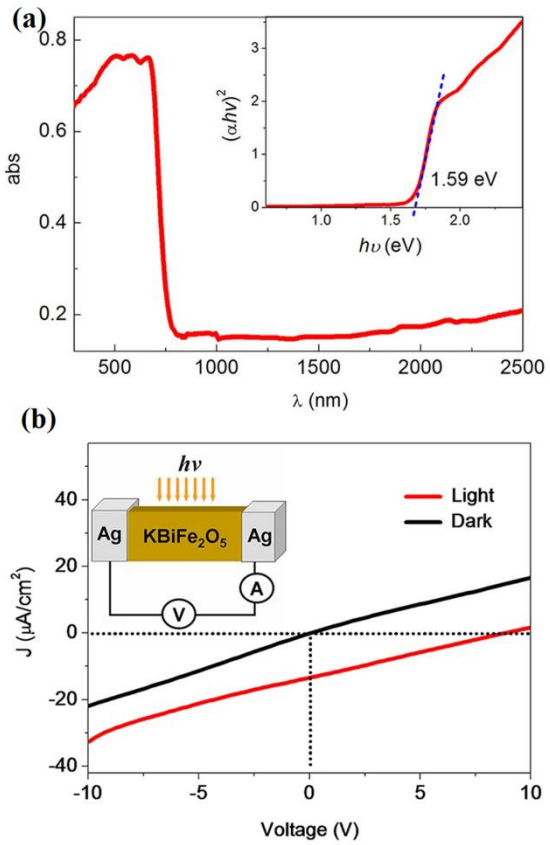

Figure 1.24 (a) Absorption spectrum of $KBiFe_2O_5$ Inset: $(\alpha hv)^2$ versus hv (b) J-V curves in the dark and under UV illumination [G. Zhang et al. (2013)].

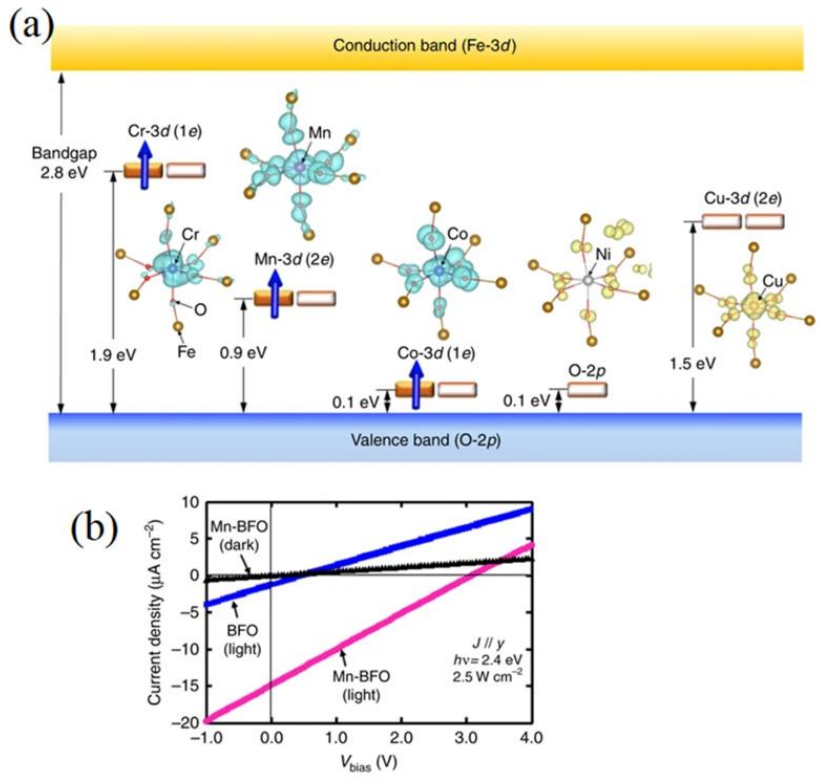

Figure 1.25 (a) schematic electronic structures of transition metal (TM=Cr, Mn, Co, Ni and Cu)-doped BFO obtained from DFT calculations (b) J–V_{bias} curve under dark and illuminated (hv=2.4 eV) conditions [H. Matsuo et al. (2017)].

1.7.2 Charge Separation in ferroelectric solar cells

In classical solar cells, when solar light is absorbed by photoactive layer of device, the mobile electron and hole pairs are generated. These electron-hole pairs are called excitons that can be separated by internal built-in-electric field. In silicon solar cells, the photo carriers are separated by the electric-field developed at p-n junction. In ferroelectric active layer based solar cells, the built-in-electric field is generated from either by Schottky junction or by ferroelectric polarization. D. Rossi et al have illustrated that the high value of ferroelectric domain polarization in material, results in well-organized charge separation and reduction in charge carriers' recombination [D. Rossi et al. (2018)]. The charge carriers are built up at the domain interfaces which causes decline in the local trap-assisted recombination process. However, in

conventional solar cells, the charge separating electric field is generated due to p-n junction or Schottky barrier effect and it depends on the band gap of solar-light absorbing layer. So, these devices depict low open circuit voltage. The devices based on ferroelectric layer as photo-absorbing layer show very high photovoltage which is generated either from bulk material, depolarization field or combination of domain walls built in fields.

Schematic charge separation processes in semiconducting p-n junction and ferroelectric active layer are illustrated in Fig.1.26. In ferroelectric layer, the self-polarized charges induce a built-in electric field which promotes the charge-separation process and prevents their recombination. The internal field in ferroelectric layer is given as

$$E = \frac{d\sigma_p}{\varepsilon_0 \varepsilon_{FEL}} \quad \ldots\ldots\ldots\ldots\ldots\ldots\ldots\ldots\ldots\ldots\ldots\ldots \quad (1.13)$$

Where 'd' is thickness of ferroelectric layer, σ_p is polarization charge density, ε_{FEL} is relative dielectric constant of ferroelectric layer, ε_0 permittivity of free space. In ferroelectric based photovoltaic devices, ferroelectric layer acts as light absorbing layer and also provides the internal electric field due to polarization. With wide band gap ferroelectric layer, the devices show very high photovoltage but low photocurrent. As discussed earlier, the observation of bulk photovoltage in non-centrosymmetric material is called bulk photovoltaic effect and explained by shift current model. According to shift current model, the charge separation process is a quantum mechanical phenomenon which is arising from the asymmetry in the electronic wave function instead of internal field [M. Nakamura et al. (2017)]. D. Kim et al have provided new approach to increase the charge separation efficiency of ferroelectric materials. The photoexcited electron-hole pairs in Cr-doped $BiFeO_3$ (BFCO) are spatially separated on Fe and Cr sites respectively, leading to low charge recombination. The positional

disordering of B-site cations in BFO increases the e-h separation efficiency and gives higher photocurrent [D. Kim et al. (2018)].

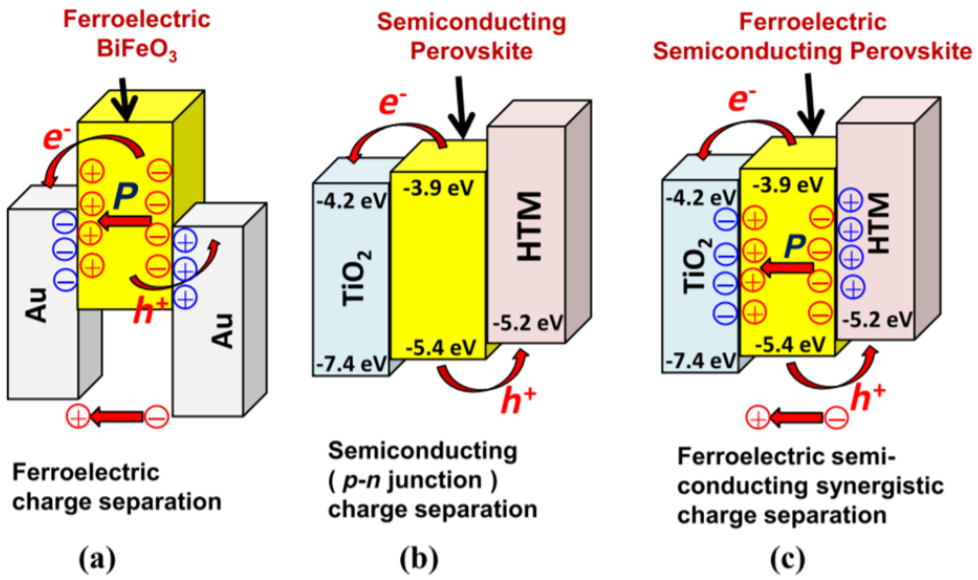

Figure 1.26 Charge separation mechanisms in (a) Ferroelectric material (b) semiconducting p-n junction (c) Ferroelectric-semiconducting perovskite heterostructure [G. A. Sewvandi et al. (2016)].

1.7.3 Charge Collection in ferroelectric solar cells

After charge separation by internal electrical field, the charges need to flow towards their respective electrodes. The electrodes must be selective to specific carriers. One electrode should be electron collecting contact while other must be a hole collecting contact so that a net directional flux of charges can be established. The charge collection efficiency depends on ferroelectric polarization of the central layer. It also depends on photo-carriers mobility and life time. Thus, thickness of central layer also plays a major role in charge collection efficiency. The charge collection efficiency can be increased by reducing the thickness of photo-absorbing layer, by replacing the metal electrode with semiconducting electrode, using combination of ferroelectric and semiconducting layers, using Pt tip as electrode for charge collection and by increasing

the depolarization field [M. Ichiki et al. (2004); B. Chen et al. (2011); Z. Fan et al. (2014); M. Alexe et al. (2011); M. Qin et al. (2007)].

B. Chen et al. have investigated the effect of top electrode on photo-response from $BiFeO_3$ based solar cells. It is reported that devices with Sn-doped In_2O_3 (ITO) as top electrode shows 25 times higher photovoltaic response than that with Au as top electrode, as shown in Fig. 1.27 [B. Chen et al. (2011)]. N. Ramakrishnegowda et al. have investigated the effect of domain walls and layer thickness on the transport properties of $Pb(Zr_{0.2}Ti_{0.8})O_3$ film. Film with thickness 75 nm shows J_{sc} ~ 0.28 mA/ cm^2 while device with 706 nm PZT layer generate J_{sc} ~ 0.16 mA/cm^2. The decrease in J_{sc} with increasing thickness (as shown in Fig. 1.28) is due to increase in path length for photo-carriers by which the recombination probability also increases [N. Ramakrishnegowda et al. (2020)].

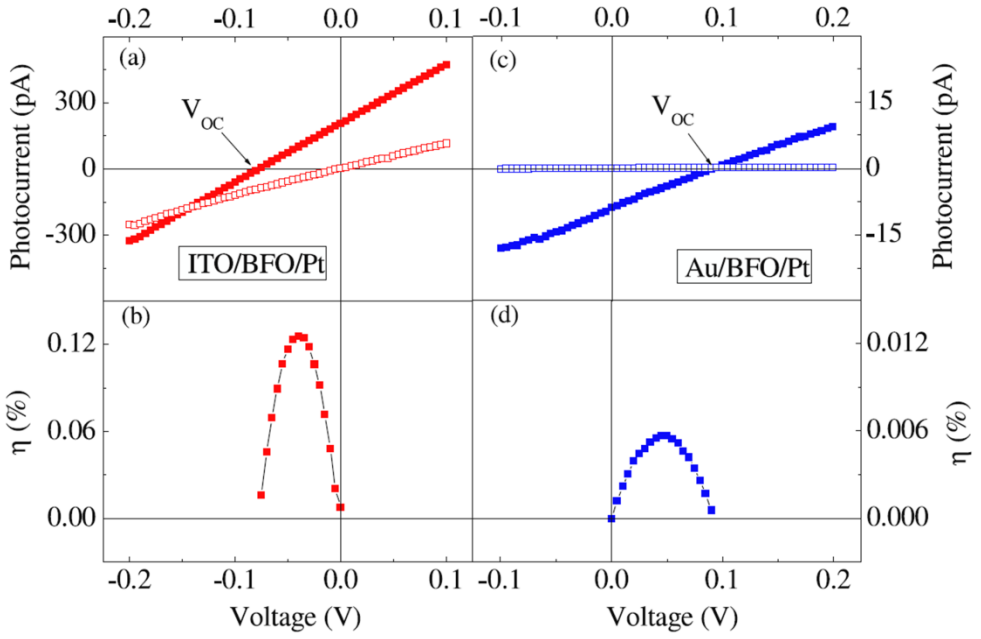

Figure 1.27 (a), (c) Current-voltage characteristics and (b), (d) power conversion efficiency η for ITO/BFO/Pt and Au/BFO/Pt, respectively, with corresponding V_{oc} dependence [B. Chen et al. (2011)].

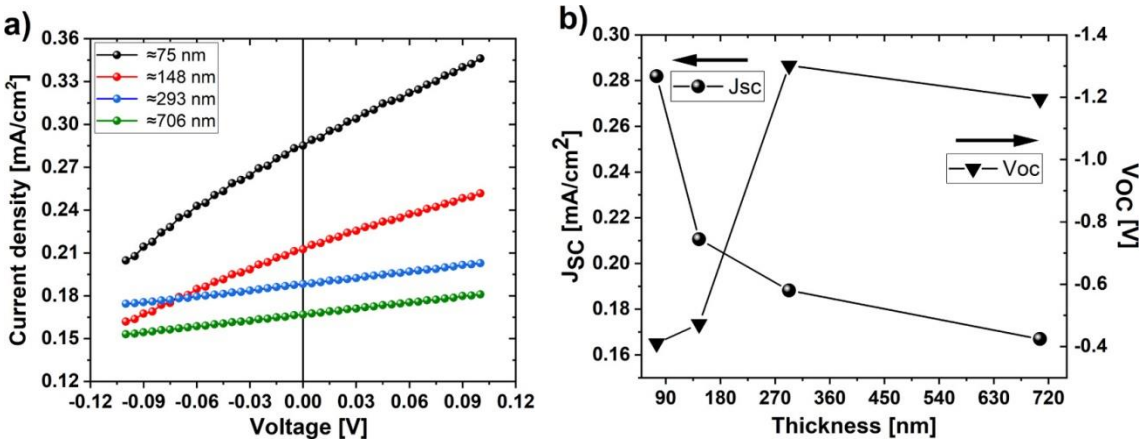

Figure 1.28 (a) J−V curve recorded under 3.06 eV at room temperature. (b) J_{SC} and V_{OC} extracted from (a) plotted with the thickness of the samples [N. Ramakrishnegowda et al. (2020)].

D. F. Pan et al. have inserted semiconducting ZnO layer between ferroelectric PZT layer and electrode and analyzed the interfacial coupling effect. As shown in Fig.1.29, the remnant polarization decreases when PZT coupled with ZnO layer is present. It is observed that photocurrent density increases from -3.345 μA/cm^2 to -42.409 μA/cm^2 for ITO/PZT/ZnO/Au as compared to ITO/PZT/Au heterostructure. Here, ZnO layer provides additional internal electrical field in the direction of depolarization field of PZT, which further promotes the photo-carrier separation [D. F. Pan et al. (2016)].

To improve the device efficiency, the p-i-n heterostructure has also been used by researchers, where ferroelectric layer is used as intrinsic layer. The hole transport layer (HTL) and electron transport layer (ETL) are used to improve the charge transport and charge collection efficiency. W. Huang et al have used Bi_2FeCrO_6 ferroelectric layer as intrinsic (i) absorber layer, NiO as p-type hole transport layer, n-type Nb-doped $SrTiO_3$ as electron transport layer. The optimized p-i-n solar cell yielded J_{sc}~ 8mA/ cm^2. The J_{sc} increased three times for p-i-n device when compared with i-n heterostructure device as depicted in Fig. 1.30 [W. Huang et al. (2017)]. M. Alexe et al. have used nanoscale top electrode to increase the charge collection efficiency and found that external quantum

efficiency is increased by up to seven orders of magnitude in $BiFeO_3$ single crystal. The nanoscale geometry of Pt- tip, causes non-uniform local electrical field below the tip. Most of the field will confine under the tip and photo carriers will drift to the electrode (tip) larger than their contact area. The corresponding I-V curve is shown in Fig.1.31 [M. Alexe et al. (2011)]. Similar photovoltaic effect is also observed in $BaTiO_3$ single crystal as shown in Fig.1.32 where 25 nm Pt-tip has been used [J. E. Spanier et al. (2016)].

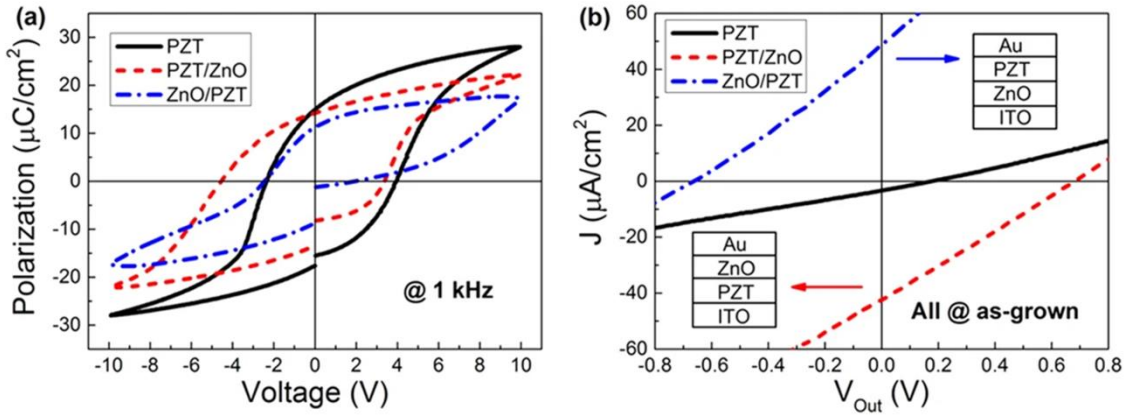

Figure 1.29 (a) Polarization-voltage hysteresis loops of the samples measured at 1 kHz. (b) Comparison of photovoltaic current density (J) vs output voltage (V_{out}) curves of the as-grown samples [D. F. Pan et al. (2016)].

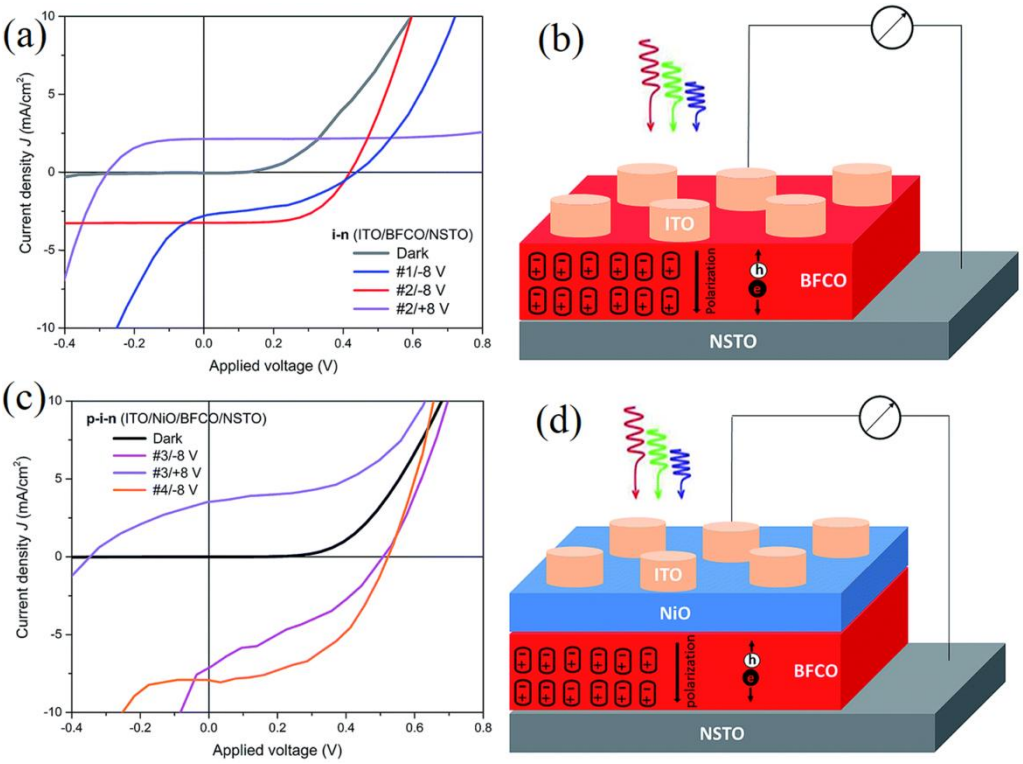

Figure 1.30 J–V characteristics under AM1.5G illumination for: (a) i–n devices and (b) p–i–n devices; Layout of the devices for: (c) i–n and (d) p–i–n [W. Huang et al. (2017)].

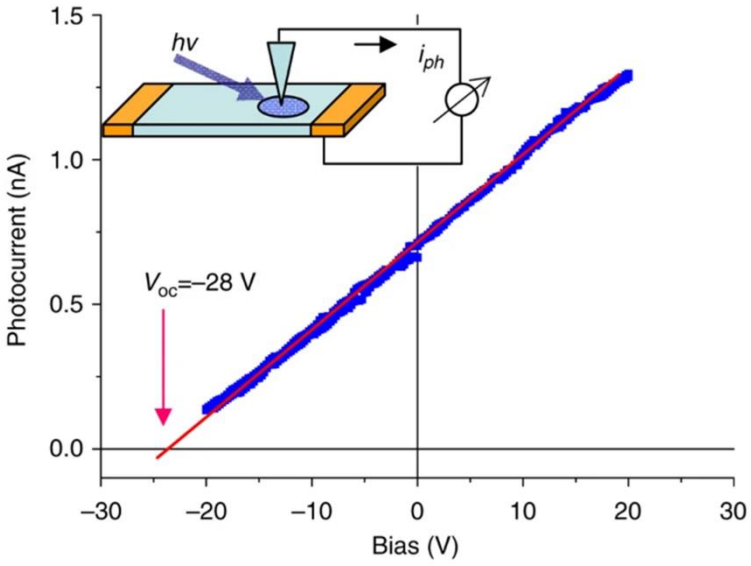

Figure 1.31 J–V characteristics measured by probing with the AFM tip in the middle of the illuminated area. The measurement setup for the local measurements by the AFM tip is also shown schematically [M Alexe et al. (2011)].

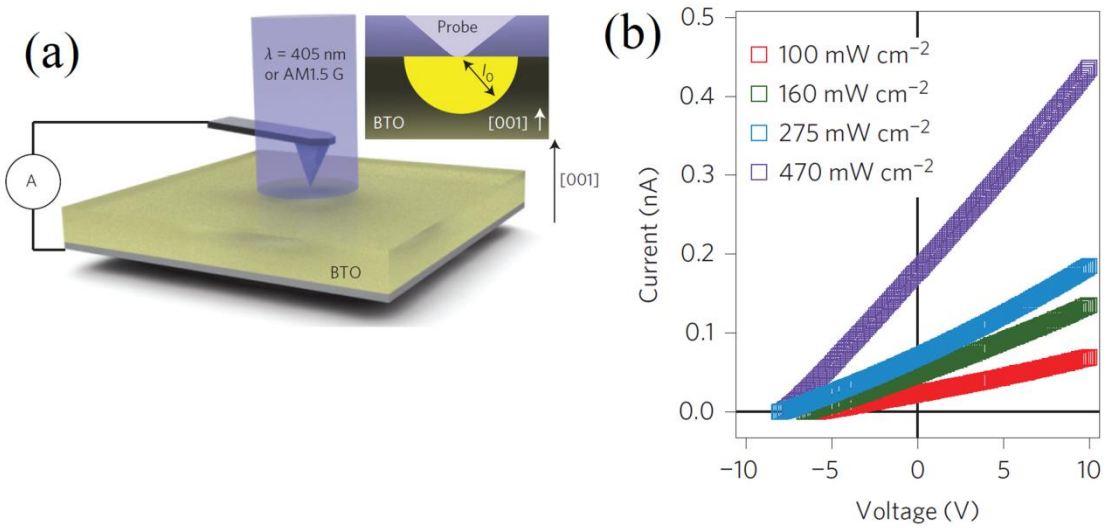

Figure 1.32 (a) The experimental configuration for I-V measurement, including the thermalization hemisphere (b) Dependence of the photovoltaic current in the BTO crystal on the intensity of the monochromatic illumination intensity using a 25-nm-radius tip [J. E. Spanier et al. (2016)].

1.8 Brief overview of ferroelectric photovoltaic materials

Recent investigations by various research groups suggest that ferroelectric oxide based photovoltaic cells have the potential to become alternative of silicon solar cells owing to their low manufacturing expenditure and outstanding stability. Ferroelectric oxide based photovoltaic cells have been centre of attention over the past ten years. Till date, variety of ferroelectric materials have been investigated that show photovoltaic effect. However, only few of them are well studied. Henceforth, we will review and discuss the photovoltaic phenomenon reported in most investigated $BiFeO_3$, $PbTiO_3$, $BaTiO_3$ and $KNbO_3$ based materials. Our focus will be on the optical as well as photovoltaic properties of these materials.

1.8.1 Bismuth Ferrite ($BiFeO_3$)

$BiFeO_3$ (BFO) a multiferroic material has emerged as a brilliant contestant for ferroelectric photovoltaic devices. It has got significant attention as multiferroic

material due to presence of room temperature ferroelectric and G-type antiferromagnetic order. BFO has very high Curie temperature (~1100K) in comparison to $PbTiO_3$ (~763K) and $BaTiO_3$ (~400 K). At room temperature, BFO shows very large spontaneous polarization (~ 100μC/cm^2). BFO belongs to ABO_3 type perovskite crystal structure. Photovoltaic devices fabricated from the absorber BFO were reported in its single crystal and epitaxial thin film form. The band gap of BFO ranges from 1.9 eV to 2.7 eV depending upon preparation method. The band gap of BFO can be easily tuned in wide range (1.5 eV – 2.1 eV) when alloyed with other elements making it suitable to absorb UV-visible range photons. C. R. Basu et al. have reported photo-response behaviour of BFO thin film but obtained very low V_{oc} [S. R. Basu et al. (2008)]. BFO shows relatively low band gap as compared to other ABO_3 ferroelectric oxides due to presence of transition metal ions with unpaired d- electrons [A. J. Hauser et al. (2008)].

Yang et al have reported PV effect in BFO thin films using $SrRuO_3$ as bottom electrode and ITO as top electrode. Fig 1.33 shows the J-V curve for this device. ITO/BFO/SRO/STO heterostructure shows V_{oc} ~ 0.8 V. The epitaxial thin films were grown by metal-organic chemical vapour deposition [S. Y. Yang et al. (2009)]. In this heterostructure, Yang et al haven't found any change in nature of I-V curve with changing the polarization direction. The single ferroelectric domain crystal of BFO has shown the switchable diode and photovoltaic effects. Fig. 1.34 (a) shows the J-E curve of BFO with Au electrodes in dark and under green light as reported by Choi et al. At zero bias, negative photo-current of 8.219 μA/cm^2 is observed. As shown in inset of Fig 1.34 (a), the obtained bulk photocurrent confirms the photovoltaic effect in BFO [T. Choi et al. (2009)]. Fig 1.34(b) shows the time dependent photocurrent at zero bias with turning the light ON and OFF.

S. Y. Yang et al. have reported above band gap voltage (16V) in epitaxial BFO film when platinum Pt electrodes were perpendicular to domain walls (71° array) as discussed earlier in section 1.6.3 and illustrated in Fig1.16 [S. Y. Yang et al. (2009)]. When electrodes were parallel to domain walls, BFO exhibit photoconductivity, but no V_{oc} is observed [Fig1.16 (d)]. In this work domain wall theory is proposed to explain the physical origin of PV effect in ferroelectric materials. The domain wall model was validated by measuring the V_{oc} with varying the number of domain walls. The strong dependence of V_{oc} on domain wall density supports this model. However, W. Ji et al. have later on experimentally illustrated PV effect in BFO due to BPVE model and concluded that both material symmetry and macroscopic electric field (depolarization field) might be important when considering the BPVE in thin films [W. Ji et al. (2010)].

Fig 1.35(a) shows the J-V curve reported by W. Ji et al. The positively poled sample shows positive photocurrent i.e., current flows out of the top electrode and vice-versa. Samples without any poling exhibit same I-V nature as for negatively poled sample. The highest V_{oc} is around 0.3V. The PV effect in unpoled BFO films is due to presence of self-polarization. The switchable PV effect indicate that ferroelectric polarization plays prominent role and internal bias field is also there due to oxygen vacancies and defects, as explained in Fig 1.35(b) [W. Ji et al. (2010)]

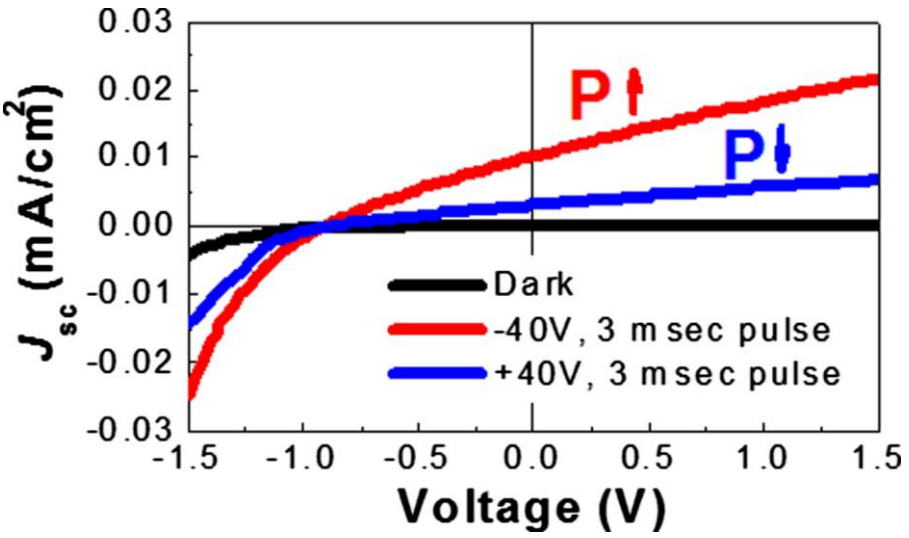

Figure 1.33 Photovoltaic effects in epitaxial BFO thin films using ITO/BFO/$SrRuO_3$/STO heterostructure [S. Y. Yang et al. (2009)].

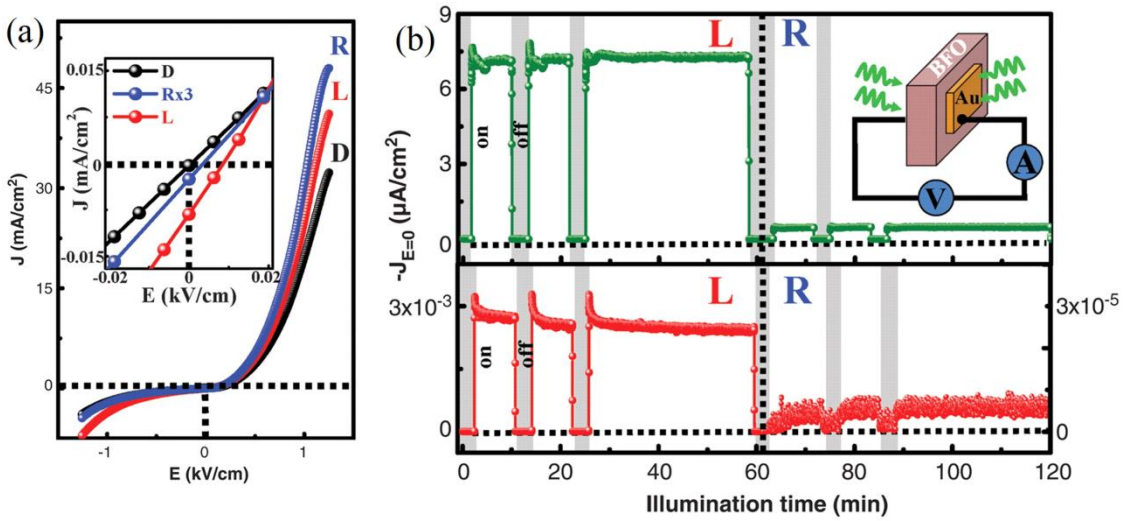

Figure 1.34 (a) J-E characteristic of the BFO sample in the dark (D) and with green-light illumination on right (R) or left (L) semitransparent Au electrodes. The inset to Fig.(a) shows an expanded view of the J-E curves near zero bias field. (b) J-t curve with (top) green light (l =532 nm) and (bottom) red light (l = 650 nm); on or off, shining on the different sides of BFO [T. Choi et al. (2009)].

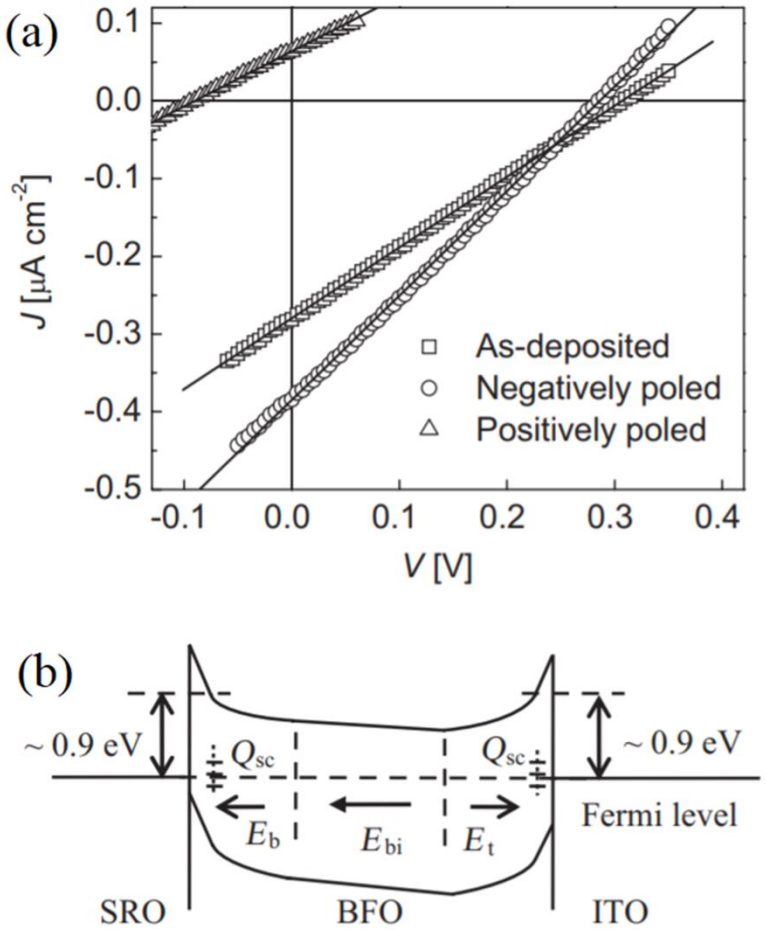

Figure 1.35 (a) Photovoltaic response for ITO/BFO/SRO/STO. (b) Schematic of energy-band alignment for the ITO/BFO/SRO capacitor. E_b and E_t are the built-in field at the bottom- and top-electrode interfaces, respectively. E_{bi} is the unswitchable built-in field in the film bulk possibly due to nonuniform distribution of defects. Q_{sc} denotes the gap-state charge density [W. Ji et al. (2010)].

1.8.2 Lead Titanate ($PbTiO_3$)

$PbTiO_3$ (PTO) is a ABO_3 type perovskite with spontaneous polarization of 0.75 C/m^2. Fridkin et al. (1978) have investigated the photoconductivity and photovoltaic current in the direction of spontaneous polarization in PTO single crystals. They have suggested possibility of existence of anomalous photovoltaic effect in PTO on the basis of observed change in photocurrent with temperature and intensity [V. M. Fridkin et al. (1978)]. K. Uchino and co-workers have reported high-voltage photovoltaic effect in $0.895PbTiO_3$-$0.105La(Zn_{2/3}Nb_{1/3})O_3$ ceramics. Fig 1.36 shows light intensity dependent I-V curve of undoped and Mn doped samples. It is observed that photovoltage saturates with increasing light intensity but current increases. The saturation of photovoltage is due to photoconductive effect [K. Uchino et al. (1983)]. J. W. Bennett et al. have theoretically predicted that Ni, Pd and Pt doped PTO solid solutions will show a reduced band gap when compared to PTO while preserving the polarization as shown in Fig.1.37.

Theoretically, Substituting the B-site of Pb-based perovskite (ABO_3) with elements whose bonds with oxygen are less ionic and more covalent should decrease the band gap. Using investigation of electronic densities of states the Ni doped PTO shows band gap ~ 0.8 eV. In PTO, conduction band is formed from O-2p orbitals and valence band is localized around Ti-3d orbitals. When Ni and O vacancies replace Ti, the Ni-d states falls in PTO band gap. The Ni-d states are localized near conduction band (C.B.) and valance band (V.B.) but are lower in energy than the Ti-3d state, thus reduce the conduction band edge relative to PTO. Thus, reduced band gap is observed for transition element doped PTO [J. W. Bennet et al. (2008)].

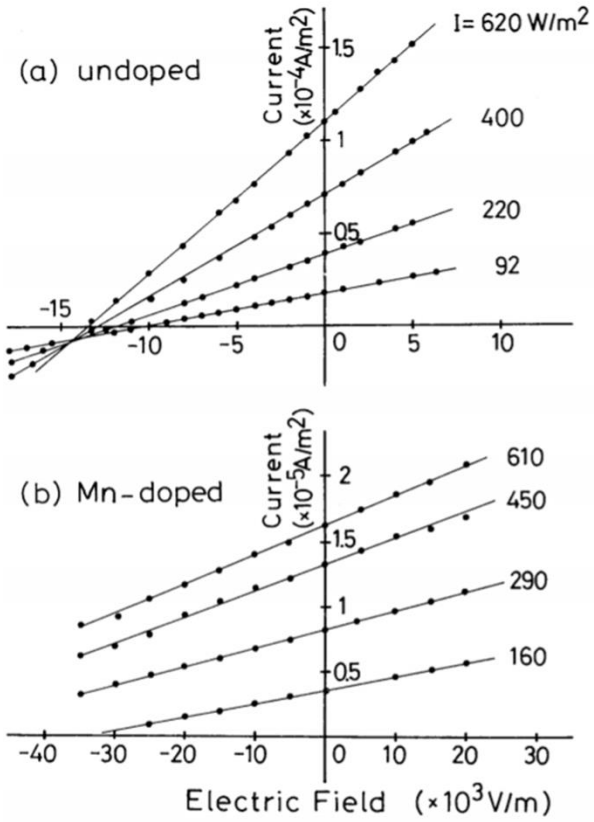

Figure 1.36 Intensity dependent I-V characteristics in (a) undoped and (b) MnO_2 Doped sample $0.895PbTiO_3$-$0.105La(Zn_{2/3}Nb_{1/3})O_3$ [K. Uchino et al. (1982)].

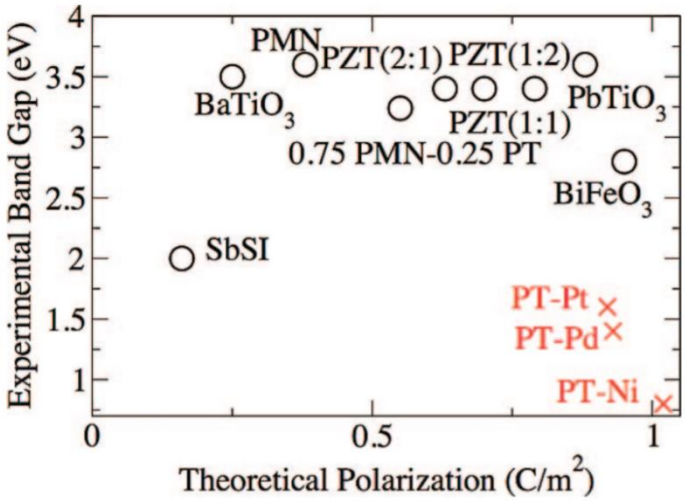

Figure 1.37 (O) Band gap of ferroelectrics materials measured experimentally and compared with their theoretical polarization (×) Estimated values of band gap for the materials proposed in this study [J. W. Bennet et al. (2008)].

G. Y. Gou et al. have used density functional theory to investigate the B-site Ni/Ti cation ordering and predicted that Ni-doped PTO system should have a direct band gap. The reduced band gap may be due to strong hybridization between Ni-d and O-p orbitals which increases Ni-O bond covalence in $Pb(Ni_xTi_{1-x})O_{3-x}$ [G. Y. Gou et al. (2011)]. Later, W. Zhou et al. have experimentally found that the band gap of PTO (3.21 eV) is reduced to 2.42 eV after Ni doping. As shown in Fig.1.38, the reduction in band gap is due to creation of new states Ni-3d-states which are lower in energy than Ti-3d states [W. Zhou et al. (2015)]. C. W. Zhao et al have prepared Ni-doped PTO thin films by sol-gel method to investigate the band gap and photocurrent. The band gap reduces to 2.86 eV for x = 0.30 composition of $PbTi_{1-x}Ni_xO_3$ thin film. The remnant polarization increases from 36.3 to 41.2 $\mu C/cm^2$ as shown in Fig.1.39. The maximum remnant polarization of 58.1 $\mu C/cm^2$ is obtained for $PbTi_{0.8}Ni_{0.2}O_3$ film. The Ni doped PTO film shows much higher photocurrent as compared to undoped PTO films as shown in Fig.1.39 (c) [C. W. Zhao et al. (2017)].

1.8.3 Solid Solution of $(1-x)Bi(Ni_{2/3}Nb_{1/3})O_3$-$xPbTiO_3$

Lead-based ferroelectric semiconductors with intricate perovskite structure have fascinated much interest due to possibility to reduce their band gap by varying the elemental composition while maintaining the high polarization. Many relaxor ferroelectric materials form binary solid-solution with $PbTiO_3$, for example $Pb(Mg_{1/3}Nb_{2/3})O_3$-$PbTiO_3$. $Pb(Ni_{1/3}Nb_{2/3})O_3$-$PbTiO_3$ etc. A morphotropic phase boundary (MPB), separating two crystallographic phase stability regions in temperature composition phase diagram, exists in all these binary solid-solution systems. The MPB is a nearly vertical phase boundary between temperature-composition phase diagram of binary solid solution separating stability region of two crystallographic phases [Ahart et

al. (2008)]. Excellent ferroelectric, dielectric and piezoelectric properties are obtained for the solid solution compositions within the MPB region.

Recently few papers have been published on the $PbTiO_3$ based binary perovskite solid solutions which show the photovoltaic effect. Solid solutions of Bismuth based ferroelectric perovskites with $PbTiO_3$, [$Bi(Me^{3+})O_3$-$PbTiO_3$] have shown higher T_c in their MPBs. $BiScO_3$-$PbTiO_3$ solid solutions shows Curie temperature around 450°C with excellent piezoelectric properties in its MPB region [R. Eitel et al. (2002); S. Zhang et al. (2003)]. $Bi(Mg_{1/2}Ti_{1/2})O_3$-$PbTiO_3$ solid solution is another materials with High T_c and high d_{33} [C. A. Randall et al. (2004); M. R. Suchomel et al. (2004)]. S. Zhang et al. [2005] have investigated a new bismuth based perovskite system (1-x)$Bi(Ni_{2/3}Nb_{1/3})O_3$-x$PbTiO_3$ (BNN-PT) with MPB region around x = 0.625 to 0.65 that separates the rhombohedral and tetragonal phases. S. Zhang et al. [2005] have shown that the structure of BNN-PT across MPB is affected by the BNN doping percentage as shown in Fig.1.40 (a). The phase diagram of BNN-PT solid solution constructed by using dielectric data is shown in Fig.1.40(b).

H. Liu et al have reported photovoltaic effect in MPB (X= 0.65) composition of BNN-PT. It is reported that the 0.65PT-0.35BNN shows a band gap of ~ 2.5 eV which decreased to ~2.3 eV with further doping of Ni. The J-V characteristics of 0.65PT-0.35BNN composition is shown in Fig.1.41. The 50μm thick ceramics pellet were sandwiched between Ag and Pt electrodes and positively and negatively poled before I-V measurements. A very high V_{oc} ~ 10V is reported. For BNN-PT, more detailed composition dependent band gap analysis is required and for higher photocurrent, the thin films of ceramics will be more useful. In view of this, in present thesis work, we have chosen this solid solution also for band gap and photovoltaic property studies.

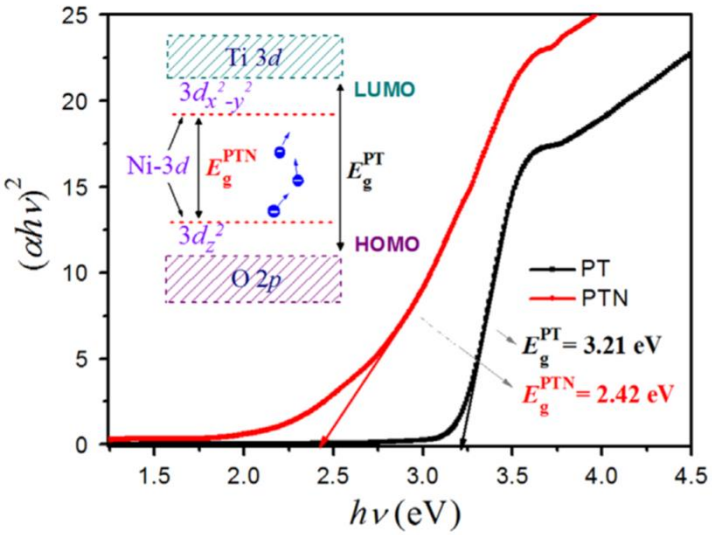

Figure 1.38 $(\alpha hv)^2$ vs hv curve for the $PbTiO_3$ (PT) and $PbTi_{0.67}Ni_{0.33}O_3$ (PTN) ceramics. The inset illustrates the mechanism of band-gap shrinkage in such type of solid solutions [W. Zhou et al. (2015)].

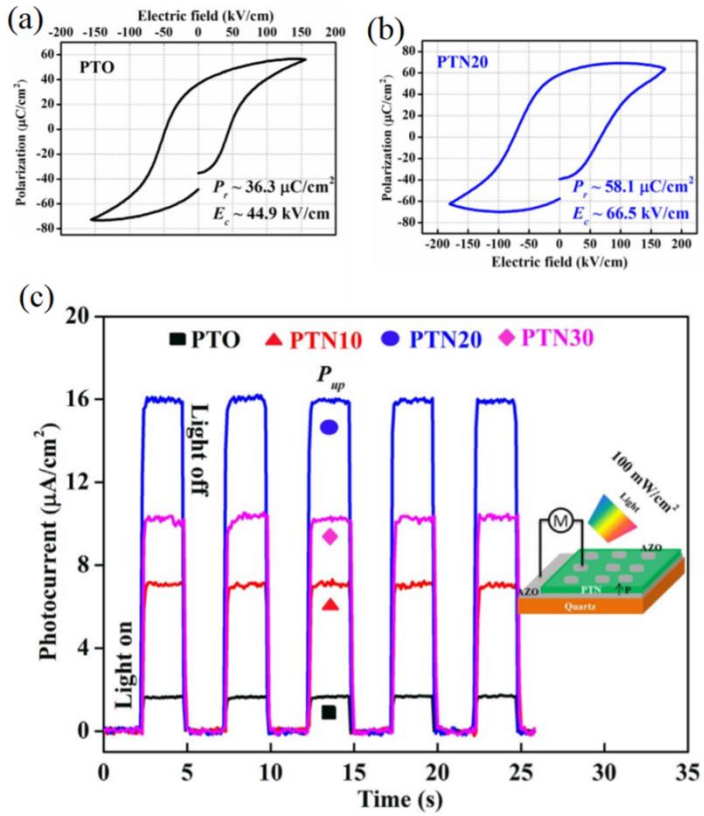

Figure 1.39 P-E loops of $PbTi_{1-x}Ni_xO_3$ (a) x=0 (b) x=0.20 thin films; (c) Composition dependent photocurrent in $PbTi_{1-x}Ni_xO_3$ thin films [C. W. Zhao et al. (2017)].

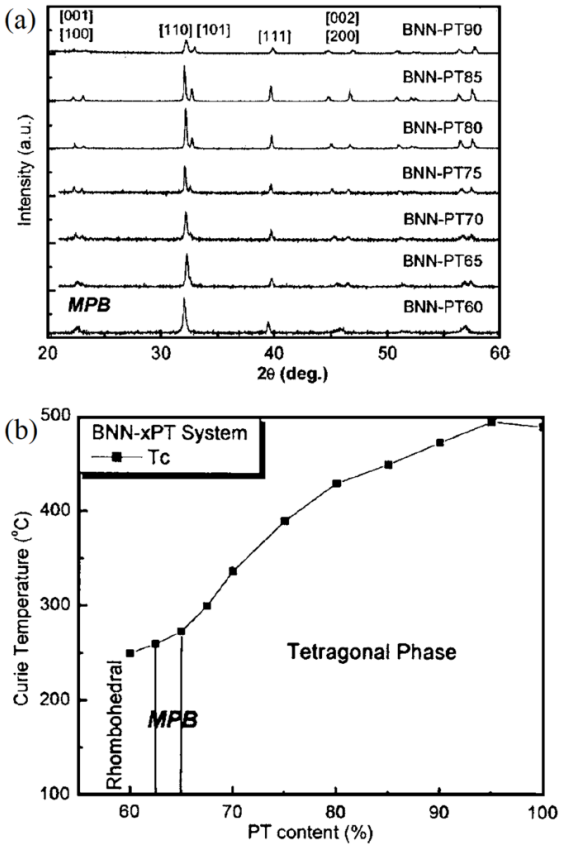

Figure 1.40 XRD patterns for (1-x)Bi($Ni_{2/3}Nb_{1/3}$)O_3-x$PbTiO_3$ with increasing PT content (b) Phase diagram showing Curie temperature [S. Zhang et al. (2005)].

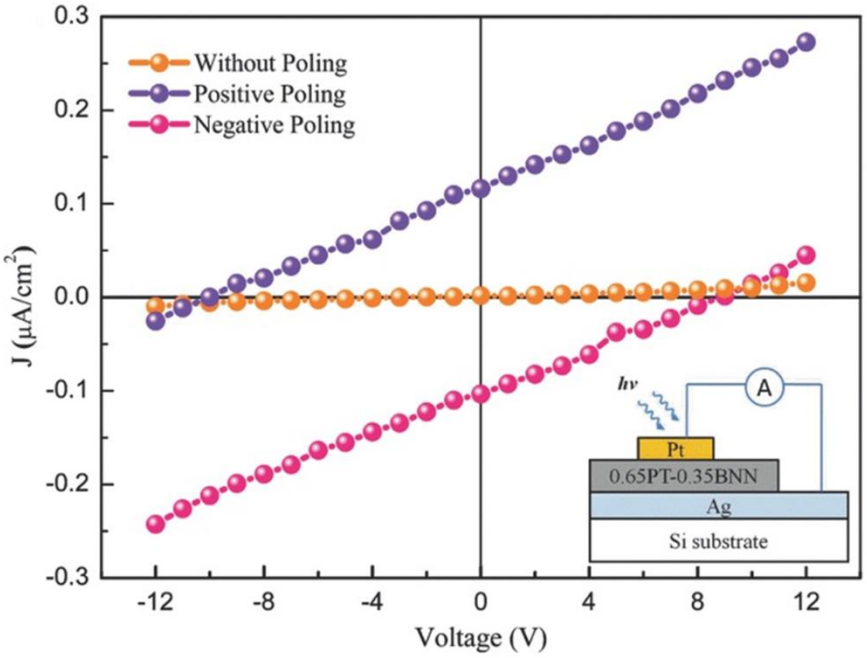

Figure 1.41 J-V curve for 0.65PT-BNN samples with and without poling, inset display device structure [H. Liu et al. (2015)].

1.8.4 Band gap engineering and PV response in $BaTiO_3$ and $KNbO_3$ based binary solid solutions

In search of lead-free materials for photovoltaic applications $BaTiO_3$ (BTO) and $KNbO_3$ were doped with transition elements to get low band gap solid solutions. Many researchers have investigated BTO for ferroelectric photovoltaic studies. D. Zheng et al. have reported that $(1-x)BaTiO_3$-$xBaCo_{0.5}Nb_{0.5}O_{3-\delta}$ exhibit low band gap (E_g~ 1.3 eV) and ferroelectric behaviour as shown in Fig.1.42 (a) [D. Zheng et al. (2019)]. The low band gap is due to presence of Co-3d states between conduction band (CB) and valence band (VB) of BTO. Similar behaviour is also reported for $(1-x)BaTiO_3$-$xBaNb_{1/3}Cr_{2/3}O_3$ ceramics which shows low band gap ~ 2.1 eV. The lowering of the band gap is attributed to presence of Cr^{3+}-3d orbitals within CB and VB of BTO [see Fig.1.42 (b), D. Zheng et al. (2020)]. L. Wu et al have reported E_g ~ 1.5 eV for $0.9BaTiO_3$-$0.1Ba(Ni_{1/2}Nb_{1/2})O_{2.75}$ ceramics showing 8 nA/cm^2 photocurrent [L. Wu et al. (2019)].

In $0.9BaTiO_3$-$0.1Ba(Ni_{1/2}Nb_{1/2})O_{2.75}$ ceramics and $(1-x)Bi(Ni_{2/3}Nb_{1/3})O_3$-$xPbTiO_3$, it is found that the band gap lowering is due to presence of Ni-3d orbitals. In view of this, we have chosen $(1-x)Bi(Ni_{2/3}Nb_{1/3})O_3$-$xBaTiO_3$ also for band gap engineering and photovoltaic study in the present thesis work. It is found that the reduction of the band gap in ABO_3 system can be achieved by transition element doping which create an additional electronic band within the CB and VB of ABO_3 system.

The $KNbO_3$ is another most extensively studied ferroelectric perovskite oxide. The solid solutions based on $KNbO_3$ has also been subject matter of photovoltaic studies. I. Greenberg et al. [2013] have reported an important low band gap solid solution system $[KNbO_3]_{1-x}$-$[Ba(Ni_{1/2}Nb_{1/2})O_{3-\delta}]_x$ (KBNNO) which show direct band gap in the range 1.1 eV-3.8 eV. Due to low band gap KBNNO can absorb 3 to 6 times more solar energy than PZT and BFO based ceramics. The Ni- containing KBNNO

solid solutions have shown band gap in the range of 1.1eV- 2.0 eV. The photovoltaic effect has been measured using 25μm KBNNO pellets with Pt and ITO electrodes. At 70K temperature, KBNNO shows V_{oc} ~ 3.5 V and J_{sc} ~ 40 nA/cm^2, as shown in Fig.1.43 [I. Grinberg et al. (2013)]. Recently, KBNNO ferroelectric have gained more attention because composition based thin films with band gap (E_g ~ 1.83eV) and P_r ~ 0.54 shows enhanced photo current J_{sc} ~ 27.3 μA/cm^2 as shown in Fig.1.44 [J. Chen et al. (2018)]. The thin film shows high P_r and High J_{sc} than that reported for bulk samples of these materials by Grinberg et al. [2019]. The increase in J_{sc} is attributed to reduced film thickness which is beneficial in reducing the charge carriers' recombination process [J. Chen et al. (2018)]

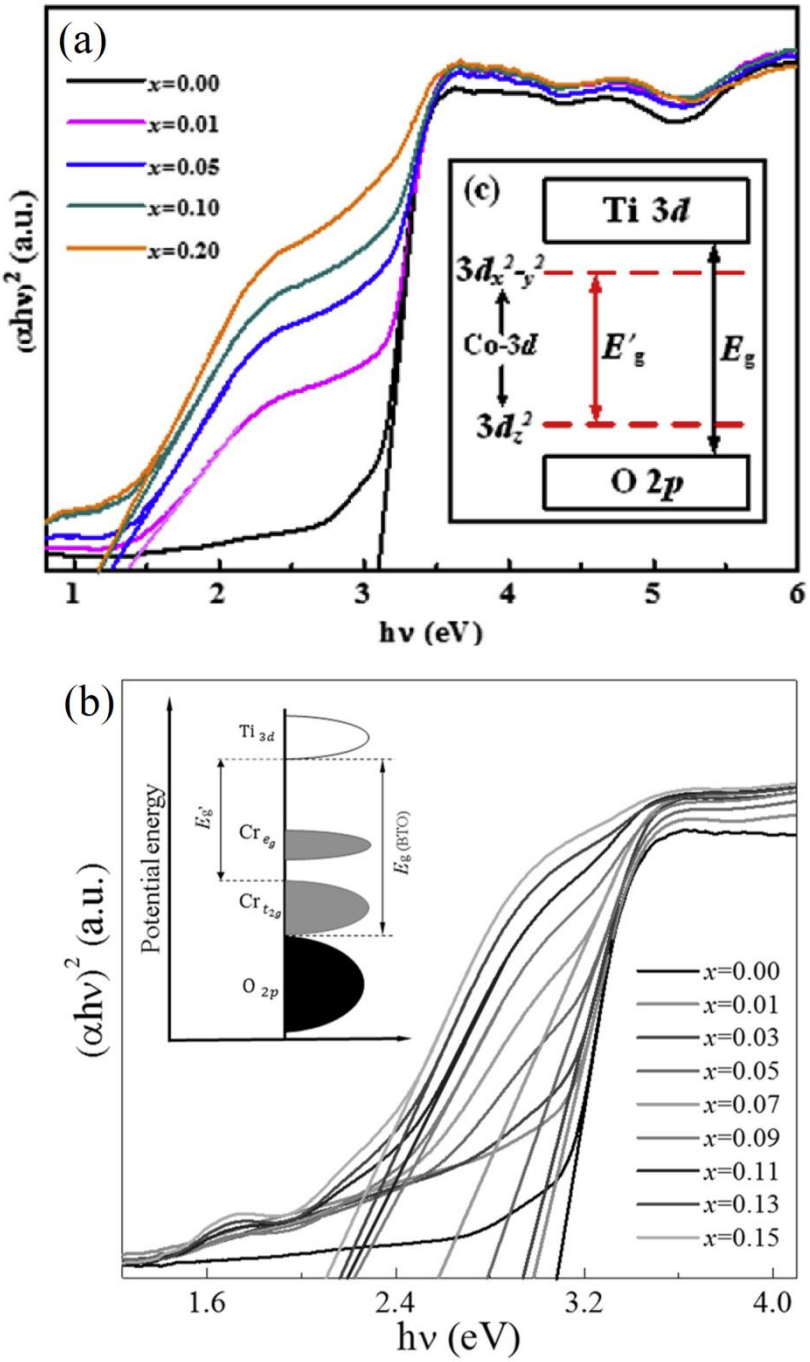

Figure 1.42 (a) plots of $(\alpha h\nu)^2$ versus hν for the absorption spectra of (1-x)$BaTiO_3$-x$BaCo_{0.5}Nb_{0.5}O_{3-\delta}$ ceramics. Inset shows the schematic diagram of band-gap structure in such materials [D. Zheng et al. (2019)]. (b) Plots of $(\alpha h\nu)^2$ vs. hν in the absorption spectra of (1-x)$BaTiO_3$-x$BaNb_{1/3}Cr_{2/3}O_{3-\delta}$ ceramics. Inset shows the schematic band structure [D. Zheng et al. (2020)].

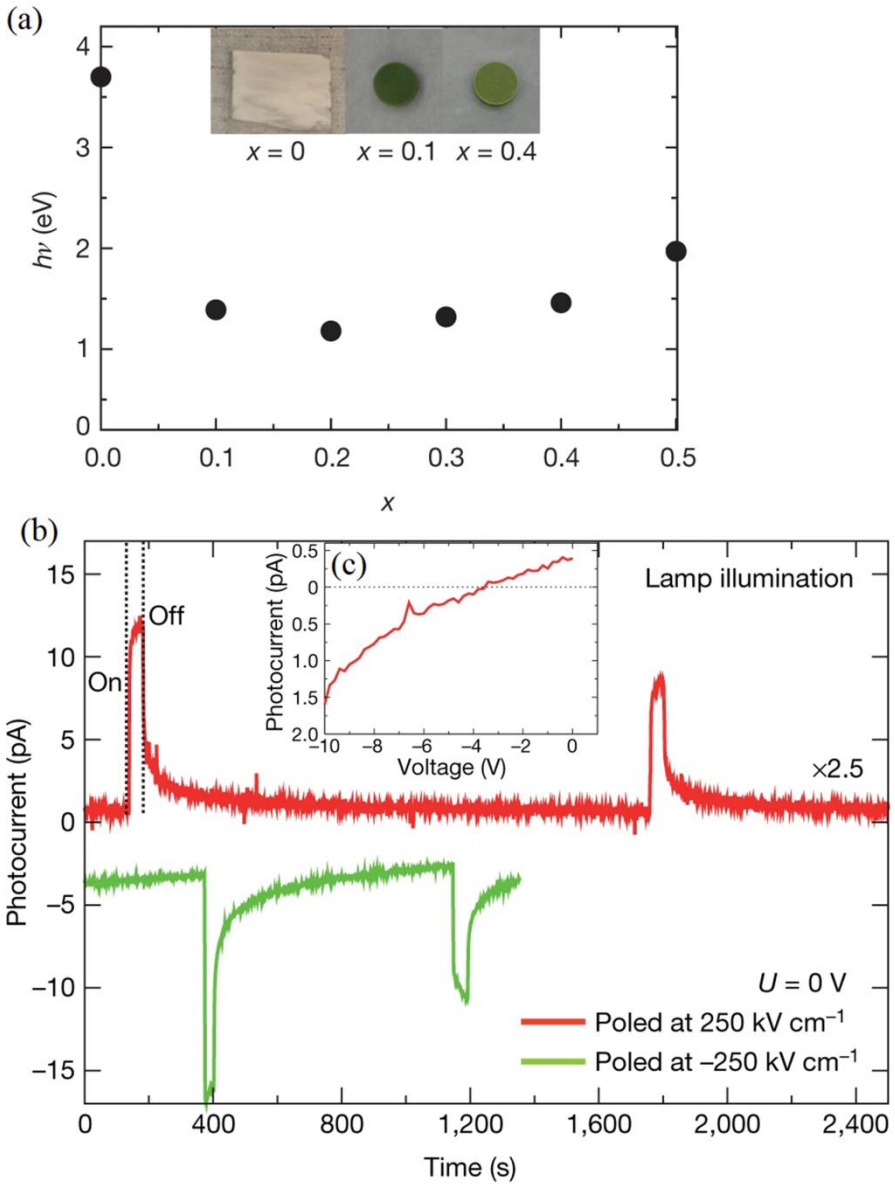

Figure 1.43 (a) Bandgap values versus BNNO fraction and Images of the $KNbO_3$, KBNNO pellets with $x = 0.1$ and $x = 0.4$ compositions. (b) Photo-response at 77 K under 4 mW/cm^2 of above-bandgap illumination. Reversal of poling voltage results in the reversal of photocurrent direction. (c) The inset shows the photo-response versus applied bias at 77 K [I. Greenberg et al. (2013)].

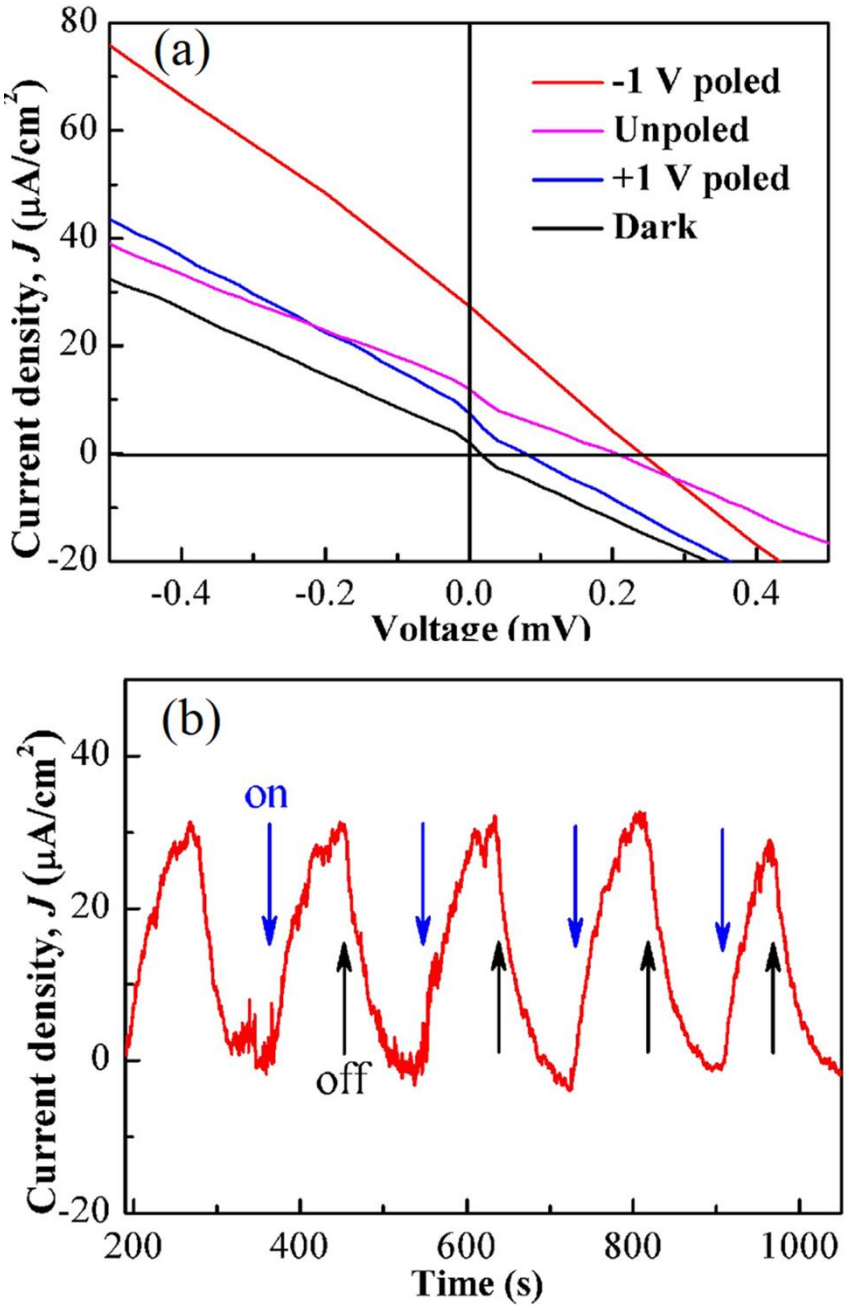

Figure 1.44 J-V characteristics of the device without poling and after poling at -1V and +1V under AM1.5 illumination, in comparison with those of the unpoled device in dark [J. Chen et al. (2018)].

1.9 Objectives of the Present Work

As discussed earlier in literature review, the band gap engineering of transition element (Ni, Nb, Co) doped $PbTiO_3$, $BaTiO_3$, $KNbO_3$ solid solution system has tremendous potential for developing technologically important photovoltaic materials. The main objectives of the present thesis work are following:

1. To optimize the synthesis conditions and to get the lowest band gap compositions of phase pure xPbTiO$_3$–(1–x)Bi(Ni$_{2/3}$Nb$_{1/3}$)O$_3$ ceramics , xPbTiO$_3$-(1-x)Bi(Co$_{1/2}$Ti$_{1/2}$)O$_3$ ceramics, xBaTiO$_3$-(1-x)Bi(Ni$_{2/3}$Nb$_{1/3}$)O$_3$ ceramics, (1-x)KNbO$_3$-xBa(Ni$_{1/2}$Nb$_{1/2}$)O$_{3-\delta}$ ceramics.

2. To study the Photo-voltaic effect in pulsed laser deposited xPbTiO$_3$–(1–x)Bi(Ni$_{2/3}$Nb$_{1/3}$)O$_3$ films

3. To analyse the charge transport properties and photovoltaic response in magnetron sputtered xPbTiO$_3$-(1-x)Bi(Co$_{1/2}$Ti$_{1/2}$)O$_3$ thin films.

4. To investigate the band gap tuning and Bulk-photovoltaic effect in xBaTiO$_3$-(1-x)Bi(Ni$_{2/3}$Nb$_{1/3}$)O$_3$ ceramics

5. To investigate the photovoltaic behaviour of magnetron sputtered and solution-processed (1-x)KNbO$_3$-xBa(Ni$_{1/2}$Nb$_{1/2}$)O$_{3-\delta}$ thin films and to study application of ZnO nano-structures as light trapping layer in ferroelectric solar cells.

The results of the above investigations are described in the subsequent chapters of this thesis.